General model and toolkit for the ionization of three or more electrons in strongly driven atoms using an effective Coulomb potential for the interaction between bound electrons

M. B. Peters, G. P. Katsoulis, and A. Emmanouilidou
Department of Physics and Astronomy, University College London, Gower Street, London WC1E 6BT, United Kingdom

(Received 31 January 2022; accepted 3 March 2022; published 5 April 2022)

We formulate a three-dimensional semiclassical model to address triple and double ionization in three-electron atoms driven by intense infrared laser pulses. During time propagation, our model fully accounts for the Coulomb singularities, the magnetic field of the laser pulse, and the motion of the nucleus at the same time as for the motion of the three electrons. The framework we develop is general and can account for multielectron ionization in strongly driven atoms with more than three electrons. To avoid unphysical autoionization arising in classical models of three or more electrons, we replace the Coulomb potential between pairs of bound electrons with effective Coulomb potentials. The Coulomb forces between electrons that are not both bound are fully accounted for. We develop a set of criteria to determine when electrons become bound during time propagation. We compare ionization spectra obtained with the model developed here and with the Heisenberg model that includes a potential term restricting an electron from closely approaching the core. Such spectra include the sum of the electron momenta along the direction of the laser field as well as the correlated electron momenta. We also compare these results with experimental ones.

DOI: 10.1103/PhysRevA.105.043102

I. INTRODUCTION

Multielectron ionization in atoms and molecules driven by intense infrared laser fields is of fundamental interest since it is mediated by electronic correlation. The theoretical study of correlated multielectron dynamics in strongly driven atoms and molecules poses a significant challenge. Indeed, three-dimensional (3D) *ab initio* quantum-mechanical methods are mostly limited to double ionization in two-electron atoms [1,2]. Various quantum-mechanical [3,4] and semiclassical techniques [5–7] that include the Coulomb singularity have been developed to address double ionization. However, for three-electron escape, due to the larger degree of complexity involved, only few theoretical studies exist that have a number of approximations. These studies include classical models with reduced dimensionality [8] and with soft core Coulomb potentials [9–13], reduced-dimensionality quantum-mechanical treatments [14–16], and semiclassical models with Heisenberg potentials [17]. On the experimental front, several studies have addressed multielectron ionization in strongly driven Ar and Ne [18–24]. For weak fields, striking angular patterns of three-electron escape and the underlying collision mechanisms were identified with 3D semiclassical models and *ab initio* quantum-mechanical techniques [25–28].

The main challenge facing quantum-mechanical studies of triple ionization in strongly driven systems is the significant amount of computational resources. This explains the development of reduced-dimensionality quantum-mechanical models [14–16]. On the other hand, the main difficulty encountered by 3D semiclassical studies of multielectron ionization that include the Coulomb singularity is unphysical autoionization. Namely, one of the bound electrons can undergo a close encounter with the core and acquire a very negative energy leading to the escape of another bound electron. This is avoided in quantum-mechanical treatments of multielectron systems due to the lower energy bound of an electron. Adding a Heisenberg potential is an approach adopted to exclude unphysical autoionization in 3D semiclassical treatments [29]. This potential amounts to adding a potential barrier that mimics the Heisenberg uncertainty principle and prevents each electron from a close encounter with the core. The addition to the Hamiltonian of an extra momentum- and position-dependent term results in the momentum of a particle being no longer directly related to the rate of change of its position, $\mathbf{p} \neq m\dot{\mathbf{r}}$ [30,31]. In what follows, we refer to this model as the H model. An advantage of this model is that electronic interactions are accounted for with Coulomb forces at all times during propagation. However, due to the Heisenberg potential, each electron accesses a reduced phase space resulting in a less accurate description of the interaction of each electron with the core. Indeed, in what follows we show that the H model gives rise to "softer" recollisions upon the return of an electron to the core.

Here, we take another approach to addressing unphysical autoionization in 3D semiclassical models that include the Coulomb singularity. We develop a 3D semiclassical model that describes the interaction between a pair of bound electrons via an effective Coulomb potential [32]. The interactions between all other pairs of electrons are described with Coulomb forces. This model advances our previous work of triple ionization in strongly driven H_2He^+, where we switched off the Coulomb force between bound electrons [33]. In the current work, we develop an efficient set of criteria to

determine on the fly, i.e., during time propagation, whether an electron is bound or "quasifree." Hence, we determine on the fly whether the interaction between two electrons is described by the Coulomb or the effective Coulomb potential. We refer to this model as ECBB—effective Coulomb potential for bound-bound electrons. We show that the ECBB model accurately describes three- and two-electron ionization spectra in strongly driven three-electron atoms.

We compare the ECBB model with the H model motivated by a recent study on the performance of different classical models concerning double ionization of strongly driven two-electron Ar in Ref. [34]. This study has shown that the two-electron classical model that includes the full Coulomb force between the two electrons [35] and the H model results in observables that agree much better with experimental results compared to the soft core Coulomb potential models.

Our motivation for developing the ECBB model is the accurate description at all times of the Coulomb interaction of each electron with the core, unlike the H model. The importance of this interaction has been demonstrated in the fingerlike structure in the correlated electron momenta in double ionization of strongly driven helium. This structure was predicted theoretically [2], observed experimentally [36,37], and explained theoretically within a classical framework [7,38]. On the other hand, the H model accurately accounts for the interaction between all pairs of electrons with Coulomb forces. The ECBB model does so for pairs of electrons where at least one electron is "quasifree." In the ECBB model the interaction between two bound electrons is described by effective Coulomb potentials and is thus less accurate. However, bound electrons have a restricted dynamics compared to "quasifree" electrons. Hence, one can argue that it is more important to accurately describe the interaction of each electron with the core rather than the interaction between bound electrons.

Here, we formulate the ECBB model and employ the H model fully accounting for both the motion of the core and all three electrons and for the magnetic field component of the Lorentz force. That is, we formulate both models in the nondipole approximation [39–41]. Thus, we can account for nondipole effects in multielectron ionization. This is unlike previous theoretical studies of strongly driven atoms which address nondipole effects mostly in single ionization. Our formalism is general and can be applied to treat multielectron ionization in more than three-electron strongly driven atoms. Here, we employ both models in the context of strongly driven Ar. We note that our 3D semiclassical model for two-electron atoms has previously yielded very good agreement with experimental observables for double ionization in strongly driven Ar driven by few-cycle laser pulses [35]. In this latter model of double ionization, we did not need to address unphysical autoionization. Moreover, we discuss in detail the differences of the ECBB and H models concerning triple- and double-ionization observables. Such spectra include the probability distribution of the sum of the electron momenta components along the direction of the laser field and the correlated electron momenta. Also, we compare our results for the sum of the momenta with experimental ones [21,22]. Finally, we obtain the probability distributions of the angle of escape between two electrons and between an electron and the core.

II. METHOD

In what follows, we describe in detail the formulation of the ECBB model and the H model that addresses multielectron escape in strongly driven atoms. The two methods resolve in a different way unphysical autoionization in 3D semiclassical models that fully account for the Coulomb singularity. In both methods, we propagate in time all three electrons and the core. Moreover, we formulate both methods in the nondipole approximation fully accounting for the magnetic field component of the laser field. The Hamiltonian of a four-body system in the nondipole approximation is given by

$$H=\sum_{i=1}^{N}\frac{[\tilde{\mathbf{p}}_i-Q_i\mathbf{A}(\mathbf{r}_i,t)]^2}{2m_i}+\sum_{i=1}^{N-1}\sum_{j=i+1}^{N}\frac{Q_iQ_j}{|\mathbf{r}_i-\mathbf{r}_j|}, \tag{1}$$

where Q_i is the charge, m_i is the mass, $\mathbf{r}_i$ is the position vector, and $\tilde{\mathbf{p}}_i$ is the canonical momentum vector of particle i. The mechanical momentum $\mathbf{p}_i$ is given by

$$\mathbf{p}_i=\tilde{\mathbf{p}}_i-Q_i\mathbf{A}(\mathbf{r}_i,t), \tag{2}$$

where $\mathbf{A}(\mathbf{r}_i,t)$ is the vector potential and $\mathbf{E}(\mathbf{r}_i,t)=-\frac{\partial\mathbf{A}(\mathbf{r}_i,t)}{\partial t}$ is the electric field. Modifying Eq. (1), in the following sections, we formulate the Hamiltonian for the ECBB and the H models. For three-electron Ar, the charge of the core is equal to $Q_1=3$ a.u. while the mass of the core is equal to $m_1=72820.8$ a.u.

A. Global regularization

In both methods, we perform a global regularization to avoid any numerical issues arising from the Coulomb singularities. For strongly driven H_2, we previously used this regularization scheme to study double and "frustrated" double ionization within the dipole approximation [42] as well as nondipole effects in nonsequential double ionization [43]. In this scheme, we define the relative position between two particles i and j as

$$\boldsymbol{\rho}_{ij}=\mathbf{r}_i-\mathbf{r}_j \tag{3}$$

and

$$\boldsymbol{\rho}_{ij}=\frac{1}{N}\left(\tilde{\mathbf{p}}_i-\tilde{\mathbf{p}}_j-\frac{m_i-m_j}{M}\langle\boldsymbol{\rho}\rangle\right), \tag{4}$$

where

$$\langle\boldsymbol{\rho}\rangle=\sum_{i=1}^{N}\tilde{\mathbf{p}}_i\quad\text{and}\quad M=\sum_{i=1}^{N}m_i. \tag{5}$$

The inverse transformation is given by

$$\mathbf{r}_i=\frac{1}{M}\sum_{j=i+1}^{N}m_j\mathbf{q}_{ij}-\frac{1}{M}\sum_{j=1}^{i-1}m_j\mathbf{q}_{ji}+\langle\mathbf{q}\rangle, \tag{6}$$

and

$$\tilde{\mathbf{p}}_i=\sum_{j=i+1}^{N}\boldsymbol{\rho}_{ij}-\sum_{j=1}^{i-1}\boldsymbol{\rho}_{ji}+\frac{m_i}{M}\langle\boldsymbol{\rho}\rangle, \tag{7}$$

where

$$\langle \mathbf{q} \rangle = \frac{1}{M} \sum_{i=1}^{N} m_i \mathbf{r}_i. \tag{8}$$

Next, we define a fictitious particle k for each pair of particles i, j as follows:

$$k(i, j) = (i-1)N - \frac{i(i+1)}{2} + j, \tag{9}$$

with $j > i$ and the total number of fictitious particles being equal to $K = N(N-1)/2$. In addition, we define the parameters α_{ik} and β_{ik} as $\alpha_{ik} = 1$, $\beta_{ik} = m_j/M$ and $\alpha_{jk} = -1$, $\beta_{jk} = -m_i/M$ when $k = k(i, j)$, otherwise $\alpha_{ik} = \beta_{ik} = 0$. Given the above, Eqs. (6) and (7) take the following simplified form:

$$\tilde{\mathbf{p}}_i = \sum_{k=1}^{K} \alpha_{ik} \boldsymbol{\rho}_k + \frac{m_i}{M} \langle \boldsymbol{\rho} \rangle \tag{10}$$

and

$$\mathbf{r}_i = \sum_{k=1}^{K} \beta_{ik} \mathbf{q}_k + \langle \mathbf{q} \rangle. \tag{11}$$

B. Heisenberg potential method

1. Description of the model

The Heisenberg potential, originally proposed by Kirschbaum and Wilets [29], is given by

$$V_{H,i} = \frac{\xi^2}{4\alpha\mu r_{i,1}^2} \exp\left\{\alpha\left[1 - \left(\frac{r_{i,1}p_{i,1}}{\xi}\right)^4\right]\right\}, \tag{12}$$

where $\mathbf{r}_{i,1} = \mathbf{r}_1 - \mathbf{r}_i$ is the relative position of each one of the three electrons $i = 2, 3, 4$ with respect to the core $i = 1$, $\mathbf{p}_{i,1}$ is the corresponding relative momentum,

$$\mathbf{p}_{i,1} = \frac{m_i \mathbf{p}_1 - m_1 \mathbf{p}_i}{m_1 + m_i}, \tag{13}$$

and $\mu = m_1 m_i/(m_i + m_1)$ is the reduced mass of the electron-core system. This potential restricts the relative position and momentum of electron i according to

$$r_{i,1} p_{i,1} \geqslant \xi. \tag{14}$$

Hence, the Heisenberg potential acts as a repulsive potential when the electron is close to the core.

2. Hamilton's equations of motion

Including the Heisenberg potential for each one of the electron-core pairs, the Hamiltonian is given by

$$H = \sum_{i=1}^{N} \frac{[\tilde{\mathbf{p}}_i - Q_i \mathbf{A}(\mathbf{r}_i, t)]^2}{2m_i} + \sum_{i=1}^{N-1} \sum_{j=i+1}^{N} \frac{Q_i Q_j}{|\mathbf{r}_i - \mathbf{r}_j|} + \sum_{i=2}^{N} V_{H,i}. \tag{15}$$

Substituting Eqs. (3) and (10) in Eq. (15), we obtain the Hamiltonian in regularized coordinates as follows:

$$H = \sum_{k,k'=1}^{K} T_{kk'} \boldsymbol{\rho}_k \boldsymbol{\rho}_{k'} + \frac{\langle \boldsymbol{\rho} \rangle^2}{2M} + \sum_{k=1}^{K} \frac{U_k}{q_k} + \sum_{i=1}^{N} \frac{Q_i^2}{2m_i} \mathbf{A}^2(\mathbf{r}_i, t) - \sum_{i=1}^{N} \frac{Q_i}{m_i} \tilde{\mathbf{p}}_i \cdot \mathbf{A}(\mathbf{r}_i, t) + \sum_{i=1}^{N-1} \frac{\xi^2}{4\alpha\mu q_i^2} \exp\left\{\alpha\left[1 - \left(\frac{q_i p_{i+1,1}}{\xi}\right)^4\right]\right\}, \tag{16}$$

where $\tilde{\mathbf{p}}$, $\mathbf{r}$ are expressed in terms of $\boldsymbol{\rho}$ and $\mathbf{q}$ via Eqs. (10) and (11). In Eq. (16), U_k is equal to $Q_i Q_j$. Using Eq. (16), we obtain Hamilton's equations of motion:

$$\begin{aligned}
\frac{d\mathbf{q}_k}{dt} &= 2\sum_{k'=1}^{K} T_{kk'} \boldsymbol{\rho}_{k'} - \sum_{i=1}^{N} \frac{Q_i}{m_i} \alpha_{ik} \mathbf{A}(\mathbf{r}_i, t) - \sum_{i=1}^{N-1} \frac{(q_i p_{i+1,1})^2}{\mu\xi^2} \frac{m_{i+1}\alpha_{1k} - m_1 \alpha_{i+1k}}{m_1 + m_{i+1}} \exp\left\{\alpha\left[1 - \left(\frac{q_i p_{i+1,1}}{\xi}\right)^4\right]\right\} \mathbf{p}_{i+1,1}, \\
\frac{d\langle \mathbf{q} \rangle}{dt} &= \frac{1}{M} \langle \boldsymbol{\rho} \rangle - \sum_{i=1}^{N} \frac{Q_i}{M} \mathbf{A}(\mathbf{r}_i, t), \\
\frac{d\boldsymbol{\rho}_k}{dt} &= \frac{U_k \mathbf{q}_k}{q_k^3} + \sum_{i=1}^{N} \frac{Q_i}{m_i} [\tilde{\mathbf{p}}_i - Q_i \mathbf{A}(\mathbf{r}_i, t)] \cdot \frac{\partial \mathbf{A}(\mathbf{r}_i, t)}{\partial \mathbf{q}_k} + \sum_{i=1}^{N-1} \left[\frac{\xi^2}{2\alpha\mu q_i^4} + \frac{(p_{i+1,1})^4}{\mu\xi^2}\right] \exp\left\{\alpha\left[1 - \left(\frac{q_i p_{i+1,1}}{\xi}\right)^4\right]\right\} \mathbf{q}_i \delta_{ik} \\
&\quad - \sum_{i=1}^{N-1} \frac{(q_i p_{i+1,1})^2}{\mu(m_1 + m_{i+1})\xi^2} \exp\left\{\alpha\left[1 - \left(\frac{q_i p_{i+1,1}}{\xi}\right)^4\right]\right\} \mathbf{p}_{i+1,1} \cdot \left[m_{i+1} Q_1 \frac{\partial \mathbf{A}(\mathbf{r}_1, t)}{\partial \mathbf{q}_k} - m_1 Q_{i+1} \frac{\partial \mathbf{A}(\mathbf{r}_{i+1}, t)}{\partial \mathbf{q}_k}\right], \\
\frac{d\langle \boldsymbol{\rho} \rangle}{dt} &= \sum_{i=1}^{N} \frac{Q_i}{m_i} [\tilde{\mathbf{p}}_i - Q_i \mathbf{A}(\mathbf{r}_i, t)] \cdot \frac{\partial \mathbf{A}(\mathbf{r}_i, t)}{\partial \langle \mathbf{q} \rangle} - \sum_{i=1}^{N-1} \frac{(q_i p_{i+1,1})^2}{\mu(m_1 + m_{i+1})\xi^2} \exp\left\{\alpha\left[1 - \left(\frac{q_i p_{i+1,1}}{\xi}\right)^4\right]\right\} \\
&\quad \times \mathbf{p}_{i+1,1} \cdot \left[m_{i+1} Q_1 \frac{\partial \mathbf{A}(\mathbf{r}_1, t)}{\partial \langle \mathbf{q} \rangle} - m_1 Q_{i+1} \frac{\partial \mathbf{A}(\mathbf{r}_{i+1}, t)}{\partial \langle \mathbf{q} \rangle}\right].
\end{aligned} \tag{17}$$

3. Propagation technique

To integrate the equations of motion in Eqs. (17), we use a leapfrog technique [44,45] jointly with the Bulirsch-Stoer method [46,47]. We have previously developed this leapfrog technique to study nondipole effects in nonsequential double ionization in strongly driven H_2 [43]. This leapfrog technique allows to solve Hamilton's equations when the derivative of the position and the momentum depends on the quantities themselves. It is an extension of the leapfrog technique we employed for strongly driven two-electron molecules in the dipole approximation [42]. In the latter case the derivative of the position and the momenta do not depend on themselves.

C. Effective Coulomb potential method

1. Derivation of the effective Coulomb potential

In what follows, we formulate a method that avoids unphysical autoionization between two bound electrons. To do so, we describe the interaction between two bound electrons with an effective Coulomb potential. However, we describe the interaction between a "quasifree" and a bound electron as well as between two quasifree electrons with the full Coulomb potential. In the next section, we define the time when an electron transitions from bound to quasifree and from quasifree to bound.

The effective Coulomb potential that electron i experiences due to the charge ζ_j of electron j, denoted by $V_{\text{eff}}(\zeta_j, |\mathbf{r}_1 - \mathbf{r}_j|)$, is derived as follows [32]. We approximate the wavefunction of a bound electron j with a $1s$ hydrogenic wavefunction

$$\psi(\zeta_j, |\mathbf{r}_1 - \mathbf{r}_j|) = \left(\frac{\zeta_j^3}{\pi}\right)^{1/2} e^{-\zeta_j |\mathbf{r}_1 - \mathbf{r}_j|}, \tag{18}$$

where the parameter ζ_j is later defined in Eq. (21). The electric charge contained within a sphere of radius r from the core is given by

$$Q(\zeta_j, r) = -\iiint |\psi(\zeta_j, r)|^2 dV, \tag{19}$$

where dV is the volume element in spherical coordinates.

Using Gauss's law, we find that the effective Coulomb potential that an electron i experiences at a distance $|\mathbf{r}_1 - \mathbf{r}_i|$ from the core due to the charge distribution of electron j is equal to (see Appendix A)

$$V_{\text{eff}}(\zeta_j, |\mathbf{r}_1 - \mathbf{r}_i|) = \frac{1 - (1 + \zeta_j |\mathbf{r}_1 - \mathbf{r}_i|) e^{-2\zeta_j |\mathbf{r}_1 - \mathbf{r}_i|}}{|\mathbf{r}_1 - \mathbf{r}_i|}. \tag{20}$$

$V_{\text{eff}}(\zeta_j, |\mathbf{r}_1 - \mathbf{r}_i|)$ is a repulsive potential which has limiting values of ζ_j when $|\mathbf{r}_1 - \mathbf{r}_i| = 0$ and zero when $|\mathbf{r}_1 - \mathbf{r}_i| \to \infty$. If the effective charge $\zeta_j(t)$ is zero then the effective potential $V_{\text{eff}}(\zeta_j, |\mathbf{r}_1 - \mathbf{r}_i|)$ is zero. The effective charge $\zeta_j(t)$, at any time during the propagation of the four-body system, is proportional to the energy $\mathcal{E}_j(t)$ of electron j, assuming electron j is bound with an energy greater than a lower limit. We set this lower limit to be equal to the ground-state energy $\mathcal{E}_{1s}$ of a hydrogenic atom with core charge equal to Q_1, i.e., $\mathcal{E}_{1s} = \frac{Q_1^2}{2}$. Moreover, when the energy of electron j, $\mathcal{E}_j(t)$, is greater than zero, we set $\zeta_j(t)$ equal to zero, while if the energy is less than the lower limit $\mathcal{E}_{1s}$ we set $\zeta_j(t)$ equal to Q_1. Hence, we define $\zeta_j(t)$ as follows:

$$\zeta_j(t) = \begin{cases} Q_1, & \mathcal{E}_j(t) \leqslant \mathcal{E}_{1s} \\ -(Q_1/\mathcal{E}_{1s})\mathcal{E}_j(t), & \mathcal{E}_{1s} < \mathcal{E}_j(t) < 0 \\ 0, & \mathcal{E}_j(t) \geqslant 0, \end{cases} \tag{21}$$

where the energy $\mathcal{E}_j(t)$ of electron j is given by

$$\mathcal{E}_j(t) = \frac{[\tilde{\mathbf{p}}_j - Q_j \mathbf{A}(\mathbf{r}_j, t)]^2}{2m_j} + \frac{Q_j Q_1}{|\mathbf{r}_1 - \mathbf{r}_j|} - Q_j \mathbf{r}_j \cdot \mathbf{E}(\mathbf{r}_j, t) + \sum_{\substack{i=2 \\ i \neq j}}^{N} c_{i,j}(t) V_{\text{eff}}(\zeta_i, |\mathbf{r}_1 - \mathbf{r}_j|). \tag{22}$$

The functions $c_{i,j}(t)$ determine whether the full Coulomb interaction or the effective $V_{\text{eff}}(\zeta_i, |\mathbf{r}_1 - \mathbf{r}_j|)$ and $V_{\text{eff}}(\zeta_j, |\mathbf{r}_1 - \mathbf{r}_i|)$ potential interactions are on or off for any pair of electrons i and j during the time propagation. Specifically, the limiting values of $c_{i,j}(t)$ are zero and 1. The value zero corresponds to the full Coulomb potential being turned on while the effective Coulomb potentials are off. This occurs for a pair of electrons i and j where either i or j is quasifree. The value 1 corresponds to the effective Coulomb potentials $V_{\text{eff}}(\zeta_i, |\mathbf{r}_1 - \mathbf{r}_j|)$ and $V_{\text{eff}}(\zeta_j, |\mathbf{r}_1 - \mathbf{r}_i|)$ being turned on while the full Coulomb potential is off. This occurs for bound electrons i and j. For simplicity, we choose $c_{i,j}(t)$ to change linearly with time between the limiting values zero and 1. Hence, $c_{i,j}(t)$ is defined as follows:

$$c_{i,j}(t) = \begin{cases} 0, & c(t) \leqslant 0 \\ c(t), & 0 < c(t) < 1 \\ 1, & c(t) \geqslant 1, \end{cases} \tag{23}$$

where $c(t) = \beta(t - t_s^{i,j}) + c_0$, and c_0 is the value of $c_{i,j}(t)$ just before a switch at time $t_s^{i,j}$. A switch at time $t_s^{i,j}$ occurs if the interaction between electrons i and j changes from full Coulomb to effective Coulomb potential or vice versa. That is, in Sec. II C 5, we discuss in detail the times an electron switches from bound to quasifree and from quasifree to bound. Every time during propagation that such a switch takes place, we check whether for each pair of electrons the full Coulomb force should be switched on and hence the effective potential switched off or the full Coulomb force should be switched off and the effective potential switched on. The former occurs if at time $t_s^{i,j}$ one of the two electrons in a pair of bound electrons changes to being quasifree while the latter occurs if in a pair of a quasifree electron and a bound electron the quasifree electron becomes bound. We clearly illustrate this in Sec. II C 5. At the start of the propagation at time t_0, $t_s^{i,j}$ is equal to t_0 and c_0 is 1 for pairs of electrons that are bound and zero otherwise. To allow for a smooth switch on or switch off of the effective Coulomb potential we choose β equal to ± 0.1; plus corresponds to a switch on and minus to a switch off of the effective Coulomb potential.

2. Derivation of the time derivative of the effective charges

Including the effective Coulomb potentials, the Hamiltonian of the four-body system is given by

$$\begin{aligned} H = &\sum_{i=1}^{N} \frac{[\tilde{\mathbf{p}}_i - Q_i \mathbf{A}(\mathbf{r}_i, t)]^2}{2m_i} + \sum_{i=2}^{N} \frac{Q_i Q_1}{|\mathbf{r}_1 - \mathbf{r}_i|} \\ &+ \sum_{i=2}^{N-1} \sum_{j=i+1}^{N} [1 - c_{i,j}(t)] \frac{Q_i Q_j}{|\mathbf{r}_i - \mathbf{r}_j|} \\ &+ \sum_{i=2}^{N-1} \sum_{j=i+1}^{N} c_{i,j}(t) [V_{\text{eff}}(\zeta_j(t), |\mathbf{r}_1 - \mathbf{r}_i|) \\ &+ V_{\text{eff}}(\zeta_i(t), |\mathbf{r}_1 - \mathbf{r}_j|)]. \end{aligned} \tag{24}$$

The dipole term $-Q_j \mathbf{r}_j \cdot \mathbf{E}(\mathbf{r}_j, t)$ of Eq. (22) involving the electric field does not appear in Hamiltonian (24). There is no contradiction. Indeed, the gauge-invariant energy of a particle does not always coincide with the gauge-dependent Hamiltonian, as discussed in Refs. [48,49]. We note that the Hamiltonian in Eq. (24) depends not only on positions, momenta, and time but also on the effective charges. Moreover, the Hamiltonian depends on time through the vector potential as well as through the effective charges that are time dependent. Since the effective charge ζ_j is proportional to the energy $\mathcal{E}_j(t)$ [see Eq. (21)], it follows that we must obtain the derivative with time of $\mathcal{E}_j(t)$. This is necessary at any time during propagation if at least two electrons are bound. To do so, we apply the chain rule in Eq. (22) and obtain

$$\begin{aligned} \dot{\mathcal{E}}_j(t) &= \frac{\partial \mathcal{E}_j(t)}{\partial \mathbf{r}_j} \cdot \dot{\mathbf{r}}_j + \frac{\partial \mathcal{E}_j(t)}{\partial \tilde{\mathbf{p}}_j} \cdot \dot{\tilde{\mathbf{p}}}_j + \frac{\partial \mathcal{E}_j(t)}{\partial \mathbf{r}_1} \cdot \dot{\mathbf{r}}_1 + \sum_{\substack{l=2 \\ l \neq j}}^{N} \frac{\partial \mathcal{E}_j(t)}{\partial \zeta_l} \dot{\zeta}_l + \frac{\partial \mathcal{E}_j(t)}{\partial t} \\ &= \frac{\partial [\mathcal{E}_j(t) - H]}{\partial \mathbf{r}_j} \cdot \dot{\mathbf{r}}_j + \frac{\partial \mathcal{E}_j(t)}{\partial \mathbf{r}_1} \cdot \dot{\mathbf{r}}_1 + \sum_{\substack{l=2 \\ l \neq j}}^{N} \frac{\partial \mathcal{E}_j(t)}{\partial \zeta_l} \dot{\zeta}_l + \frac{\partial \mathcal{E}_j(t)}{\partial t}, \\ &= \frac{\partial \left[-Q_j \mathbf{r}_j \cdot \mathbf{E}(\mathbf{r}_j, t) - \sum_{i=2}^{N-1} \sum_{m=i+1}^{N} [1 - c_{i,m}(t)] \frac{Q_i Q_m}{|\mathbf{r}_i - \mathbf{r}_m|} \right]}{\partial \mathbf{r}_j} \cdot \dot{\mathbf{r}}_j + \left[-\frac{Q_1 Q_j (\mathbf{r}_1 - \mathbf{r}_j)}{|\mathbf{r}_1 - \mathbf{r}_j|^3} + \sum_{\substack{i=2 \\ i \neq j}}^{N} c_{i,j}(t) \frac{\partial V_{\text{eff}}(\zeta_i, |\mathbf{r}_1 - \mathbf{r}_j|)}{\partial \mathbf{r}_1} \right] \cdot \dot{\mathbf{r}}_1 \\ &+ \sum_{\substack{i=2 \\ i \neq j}}^{N} c_{i,j}(t) \frac{\partial V_{\text{eff}}(\zeta_i, |\mathbf{r}_1 - \mathbf{r}_j|)}{\partial \zeta_i} \dot{\zeta}_i + \sum_{\substack{i=2 \\ i \neq j}}^{N} \dot{c}_{i,j}(t) V_{\text{eff}}(\zeta_i, |\mathbf{r}_1 - \mathbf{r}_j|) + Q_j \dot{\mathbf{r}}_j \cdot \mathbf{E}(\mathbf{r}_j, t) - Q_j \mathbf{r}_j \cdot \frac{\partial \mathbf{E}(\mathbf{r}_j, t)}{\partial t} \\ &= \sum_{i=2}^{N-1} \sum_{m=i+1}^{N} [1 - c_{i,m}(t)] \frac{Q_i Q_m (\mathbf{r}_i - \mathbf{r}_m)}{|\mathbf{r}_i - \mathbf{r}_m|^3} (\delta_{i,j} - \delta_{m,j}) \cdot \dot{\mathbf{r}}_j + \left[-\frac{Q_1 Q_j (\mathbf{r}_1 - \mathbf{r}_j)}{|\mathbf{r}_1 - \mathbf{r}_j|^3} + \sum_{\substack{i=2 \\ i \neq j}}^{N} c_{i,j}(t) \frac{\partial V_{\text{eff}}(\zeta_i, |\mathbf{r}_1 - \mathbf{r}_j|}{\partial \mathbf{r}_1} \right] \cdot \dot{\mathbf{r}}_1 \\ &+ \sum_{\substack{i=2 \\ i \neq j}}^{N} \left[c_{i,j}(t) \frac{\partial V_{\text{eff}}(\zeta_i, |\mathbf{r}_1 - \mathbf{r}_j|)}{\partial \zeta_i} \dot{\zeta}_i + \dot{c}_{i,j}(t) V_{\text{eff}}(\zeta_i, |\mathbf{r}_1 - \mathbf{r}_j|) \right] - Q_j \mathbf{r}_j \cdot \dot{\mathbf{E}}(\mathbf{r}_j, t), \end{aligned} \tag{25}$$

where we use $\dot{\mathbf{r}}_j = \frac{\partial \mathcal{E}_j(t)}{\partial \tilde{\mathbf{p}}_j}$ and $\dot{\tilde{\mathbf{p}}}_j = -\frac{\partial H}{\partial \mathbf{r}_j}$. The above expression can be finally written as

$$\dot{\mathcal{E}}_j(t) = f_j + \sum_{\substack{i=2 \\ i \neq j}}^{N} c_{i,j}(t) \frac{\partial V_{\text{eff}}(\zeta_i, |\mathbf{r}_1 - \mathbf{r}_j|)}{\partial \zeta_i} \dot{\zeta}_i, \tag{26}$$

where $f_j(\mathbf{r}, \mathbf{p}, t, \mathcal{E})$ are all the terms in Eq. (25) that do not depend on $\dot{\zeta}_i(t)$. The time derivative of ζ_i is given by

$$\dot{\zeta}_i = \begin{cases} 0, & \mathcal{E}_i(t) \leqslant \mathcal{E}_{1s} \\ -(Q_1/\mathcal{E}_{1s}) \dot{\mathcal{E}}_i(t), & \mathcal{E}_{1s} < \mathcal{E}_i(t) < 0 \\ 0, & \mathcal{E}_i(t) \geqslant 0. \end{cases} \tag{27}$$

We obtain an equation similar to Eq. (26) for each electron. Hence, at any time during propagation, we solve a system of equations to obtain the derivative in time of the energies of each electron. As a result, we express each $\dot{\mathcal{E}}$ as a function of $(\mathbf{r}, \mathbf{p}, t, \mathcal{E})$ with no dependence on the derivatives of the energies.

3. Hamilton's equations of motion

Substituting Eqs. (3) and (10) in Eq. (24), we find the Hamiltonian in regularized coordinates to be given by

$$H = \sum_{k,k'=1}^{K} T_{kk'}\boldsymbol{\rho}_k\boldsymbol{\rho}_{k'} + \frac{\langle\boldsymbol{\rho}\rangle^2}{2M} + \sum_{k=1}^{K}[1-c_k(t)]\frac{U_k}{q_k} + \sum_{i=1}^{N}\frac{Q_i^2}{2m_i}\mathbf{A}^2(\mathbf{r}_i,t) - \sum_{i=1}^{N}\frac{Q_i}{m_i}\tilde{\mathbf{p}}_i\cdot\mathbf{A}(\mathbf{r}_i,t) + \sum_{k=1}^{K}c_k(t)V_k, \tag{28}$$

where

$$V_{k(i,j)} = V_{\text{eff}}(\zeta_j, |\mathbf{r}_1-\mathbf{r}_i|) + V_{\text{eff}}(\zeta_i, |\mathbf{r}_1-\mathbf{r}_j|), \tag{29}$$

and $\tilde{\mathbf{p}}$, $\mathbf{r}$ are expressed in terms of $\boldsymbol{\rho}$ and $\mathbf{q}$ via Eqs. (10) and (11). Moreover, for $k=1,2,3$, $\mathbf{q}_k$ corresponds to the relative distance between each one of the three electrons and the core. Since the Coulomb force between each of the three electrons and the core is always on, we set $c_k(t)=0$, for $k=1,2,3$. Using Eq. (28), we find that Hamilton's equations of motion are given by

$$\begin{aligned}
\frac{d\mathbf{q}_k}{dt} &= 2\sum_{k'=1}^{K}T_{kk'}\boldsymbol{\rho}_{k'} - \sum_{i=1}^{N}\frac{Q_i}{m_i}\alpha_{ik}\mathbf{A}(\mathbf{r}_i,t),\\
\frac{d\langle\mathbf{q}\rangle}{dt} &= \frac{1}{M}\langle\boldsymbol{\rho}\rangle - \sum_{i=1}^{N}\frac{Q_i}{M}\mathbf{A}(\mathbf{r}_i,t),\\
\frac{d\boldsymbol{\rho}_k}{dt} &= [1-c_k(t)]\frac{U_k\mathbf{q}_k}{q_k^3} - \sum_{k'=1}^{K}c_{k'}(t)\frac{\partial V_{k'}}{\partial\mathbf{q}_k} + \sum_{i=1}^{N}\frac{Q_i}{m_i}[\tilde{\mathbf{p}}_i - Q_i\mathbf{A}(\mathbf{r}_i,t)]\cdot\frac{\partial\mathbf{A}(\mathbf{r}_i,t)}{\partial\mathbf{q}_k},\\
\frac{d\langle\boldsymbol{\rho}\rangle}{dt} &= \sum_{i=1}^{N}\frac{Q_i}{m_i}[\tilde{\mathbf{p}}_i - Q_i\mathbf{A}(\mathbf{r}_i,t)]\cdot\frac{\partial\mathbf{A}(\mathbf{r}_i,t)}{\partial\langle\mathbf{q}\rangle},
\end{aligned} \tag{30}$$

where

$$\frac{\partial V_{k'(i,j)}}{\partial\mathbf{q}_k} = \frac{\partial V_{k'}}{\partial\mathbf{q}_k}\delta_{k,k(1,i)} + \frac{\partial V_{k'}}{\partial\mathbf{q}_k}\delta_{k,k(1,j)}, \tag{31}$$

where $\tilde{\mathbf{p}}, \mathbf{r}$ are expressed in terms of $\boldsymbol{\rho}$ and $\mathbf{q}$ via Eqs. (10) and (11). From Eqs. (30) and (31) it follows that the term $\sum_{k'=1}^{K}c_{k'}(t)\frac{\partial V_{k'}}{\partial\mathbf{q}_k}$ is nonzero for $k=1,2,3$ and has the following form:

$$\begin{aligned}
\sum_{k'=1}^{K}c_{k'}(t)\frac{\partial V_{k'}}{\partial\mathbf{q}_1} &= c_4(t)\frac{\partial V_{\text{eff}}(\zeta_3,|\mathbf{r}_1-\mathbf{r}_2|)}{\partial\mathbf{q}_1} + c_5(t)\frac{\partial V_{\text{eff}}(\zeta_4,|\mathbf{r}_1-\mathbf{r}_2|)}{\partial\mathbf{q}_1}\\
&= c_4(t)\frac{-1+[1+2\zeta_3q_1(1+\zeta_3q_1)]e^{-2\zeta_3q_1}}{q_1^3}\mathbf{q}_1 + c_5(t)\frac{-1+[1+2\zeta_4q_1(1+\zeta_4q_1)]e^{-2\zeta_4q_1}}{q_1^3}\mathbf{q}_1,\\
\sum_{k'=1}^{K}c_{k'}(t)\frac{\partial V_{k'}}{\partial\mathbf{q}_2} &= c_4(t)\frac{\partial V_{\text{eff}}(\zeta_2,|\mathbf{r}_1-\mathbf{r}_3|)}{\partial\mathbf{q}_2} + c_6(t)\frac{\partial V_{\text{eff}}(\zeta_4,|\mathbf{r}_1-\mathbf{r}_3|)}{\partial\mathbf{q}_2}\\
&= c_4(t)\frac{-1+[1+2\zeta_2q_2(1+\zeta_2q_2)]e^{-2\zeta_2q_2}}{q_2^3}\mathbf{q}_2 + c_6(t)\frac{-1+[1+2\zeta_4q_2(1+\zeta_4q_2)]e^{-2\zeta_4q_2}}{q_2^3}\mathbf{q}_2,\\
\sum_{k'=1}^{K}c_{k'}(t)\frac{\partial V_{k'}}{\partial\mathbf{q}_3} &= c_5(t)\frac{\partial V_{\text{eff}}(\zeta_2,|\mathbf{r}_1-\mathbf{r}_4|)}{\partial\mathbf{q}_3} + c_6(t)\frac{\partial V_{\text{eff}}(\zeta_3,|\mathbf{r}_1-\mathbf{r}_4|)}{\partial\mathbf{q}_3}\\
&= c_5(t)\frac{-1+[1+2\zeta_2q_3(1+\zeta_2q_3)]e^{-2\zeta_2q_3}}{q_3^3}\mathbf{q}_3 + c_6(t)\frac{-1+[1+2\zeta_3q_3(1+\zeta_3q_3)]e^{-2\zeta_3q_3}}{q_3^3}\mathbf{q}_3.
\end{aligned}$$

In addition to Eq. (30), we have three more equations for $\dot{\mathcal{E}}(\mathbf{q},\boldsymbol{\rho},t,\mathcal{E})$.

4. Propagation technique

In our formulation, we fully account for the Coulomb singularities. Hence, an electron can approach infinitely close to the nucleus during time propagation. To ensure the accurate numerical treatment of the N-body problem in the laser field, we perform a global regularization. This regularization was introduced in the context of the gravitational N-body problem [50]. Here, we integrate the equations of motion using a leapfrog technique [44,45] jointly with the Bulirsch-Stoer method [46,47]. This leapfrog technique allows integration of

Hamilton's equation when the derivatives of the positions and the momenta depend on the quantities themselves. We previously employed this technique in our studies of nondipole effects in nonsequential double ionization of strongly driven H_2 [43]. The difference between the leapfrog technique employed in this work and the one previously employed in Ref. [43] is that the former is more involved. Indeed, in the current leapfrog technique we also need to propagate in time the energies $\mathcal{E}(t)$ [see Eq. (25)]. The steps involved in this leapfrog technique are as follows.

First, we perform a time transformation $t \to s$, where

$$ds = \Omega(\mathbf{q})dt, \tag{32}$$

with $\Omega(\mathbf{q})$ an arbitrary positive function of $\mathbf{q}$. We select the function

$$\Omega(\mathbf{q}) = \sum_{k=1}^{K} \frac{1}{|\mathbf{q}_k|}, \tag{33}$$

which forces the time step to decrease when two particles undergo a close encounter and to increase when all particles are far away from each other. The equations of motion now take the following form:

$$\begin{aligned} \mathbf{q}' &= \dot{\mathbf{q}}(\mathbf{q}, \boldsymbol{\rho}, t)/\Omega(\mathbf{q}), \\ \boldsymbol{\rho}' &= \dot{\boldsymbol{\rho}}(\mathbf{q}, \boldsymbol{\rho}, t, \mathcal{E})/\Omega(\mathbf{q}), \\ t' &= 1/\Omega(\mathbf{q}), \\ \mathcal{E}' &= \dot{\mathcal{E}}(\mathbf{q}, \boldsymbol{\rho}, t, \mathcal{E})/\Omega(\mathbf{q}), \end{aligned} \tag{34}$$

with prime denoting the derivative with respect to the new variable s. The integration is based on the leapfrog technique described in Ref. [43] that introduces four auxiliary variables, two vectors $\mathbf{W^q}$, $\mathbf{W}^{\boldsymbol{\rho}}$ and two scalars W^t, $W^{\mathcal{E}}$. As a result, an extended system is obtained where the derivatives of the position, the momenta, and the energies no longer depend on the quantities themselves. The extended equations are given by

$$\begin{aligned} \mathbf{q}' &= \dot{\mathbf{q}}(\mathbf{W^q}, \boldsymbol{\rho}, W^t)/\Omega(\mathbf{W^q}), \\ \mathbf{W}^{\boldsymbol{\rho}\prime} &= \dot{\boldsymbol{\rho}}(\mathbf{W^q}, \boldsymbol{\rho}, W^t, \mathcal{E})/\Omega(\mathbf{W^q}), \\ t' &= 1/\Omega(\mathbf{W^q}), \\ W^{\mathcal{E}\prime} &= \dot{\mathcal{E}}(\mathbf{W^q}, \boldsymbol{\rho}, W^t, \mathcal{E})/\Omega(\mathbf{W^q}), \end{aligned}$$

and

$$\begin{aligned} \mathbf{W^q}' &= \dot{\mathbf{q}}(\mathbf{q}, \mathbf{W}^{\boldsymbol{\rho}}, t)/\Omega(\mathbf{q}), \\ \boldsymbol{\rho}' &= \dot{\boldsymbol{\rho}}(\mathbf{q}, \mathbf{W}^{\boldsymbol{\rho}}, t, W^{\mathcal{E}})/\Omega(\mathbf{q}), \\ W^{t'} &= 1/\Omega(\mathbf{q}), \\ \mathcal{E}' &= \dot{\mathcal{E}}(\mathbf{q}, \mathbf{W}^{\boldsymbol{\rho}}, t, W^{\mathcal{E}})/\Omega(\mathbf{q}). \end{aligned}$$

We propagate for a time step by propagating for half a step each quadruplet of variables $(\mathbf{q}, \mathbf{W}^{\boldsymbol{\rho}}, \mathrm{t}, \mathrm{W}^{\mathcal{E}})$ and $(\mathbf{W^q}, \boldsymbol{\rho}, W^t, \mathcal{E})$ in an alternating way; see the leapfrog algorithm described in Appendix B. Moreover, to achieve better accuracy, we incorporate the leapfrog method in the Bulirsch-Stoer extrapolation scheme [46,47]. In this scheme, a propagation over a step H is split into n substeps of size $h = H/n$. We use the leapfrog method to propagate over each substep. In Fig. 1, we offer a schematic illustration of the propagation during a time substep of size h. The detailed algorithm is described in Appendix B. This process is repeated with increasing number of substeps, i.e., $n \to \infty$, until an extrapolation with a satisfactory error is achieved.

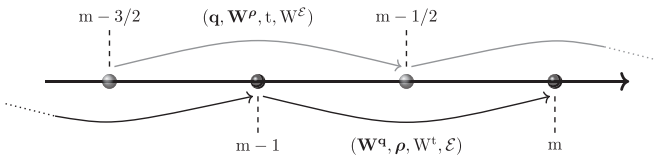

FIG. 1. Schematic illustration of the propagation of the two quadruplets $(\mathbf{q}, \mathbf{W}^{\boldsymbol{\rho}}, t, W^{\mathcal{E}})$ and $(\mathbf{W^q}, \boldsymbol{\rho}, W^t, \mathcal{E})$ over a substep of size h, $m - 3/2 \to m - 1/2$ and $m - 1 \to m$, respectively, with $m = 2, \ldots, n - 1$.

5. *Definition of quasifree and bound electron*

In the ECBB model the interaction between a pair of electrons where at least one is quasifree is described with Coulomb forces. The interaction between bound electrons is described with effective Coulomb potentials. Hence, we need to define during time propagation, i.e., on the fly, if an electron is quasifree or bound. At the start of propagation, the electron that tunnel ionizes (electron 2) is considered quasifree and the other two (electrons 3 and 4) are bound. We denote the core as particle 1.

At times $t > t_0$, a quasifree electron i transitions to bound if the following conditions are satisfied: (i) the magnitude of the potential of electron i with the core, $V_{i,c}$, is larger than a threshold value, i.e., $V_{i,c} > V_{\min}$ at t_1, and $V_{i,c}$ is continuously increasing, i.e., $\frac{dV_{i,c}(t_{n+5})}{dt} > \frac{dV_{i,c}(t_n)}{dt}$ for five times t_n which are five time steps apart with the first one being at time t_1 [see Fig. 2(a)]; (ii) the position of electron i along the electric field, i.e., z axis here, has at least two extrema of the same kind, i.e., two maxima or two minima, in a time interval less than half a period of the laser field. At the time when the second extremum is identified in the position of electron i along the electric field, electron i becomes bound. This time is a switch time $t_s^{i,j}$ if there is an electron j which is also bound (see black solid line in the plot of $c_{i,j}$ as a function of time in Fig. 2). That is, the full Coulomb force between electrons i and j starts to be switched off and the effective potentials start to be switched on. We start checking if condition (ii) is satisfied at time t_2 when electron i has the closest approach to the core, i.e., $V_{i,c}$ is maximum. We stop checking whether condition (ii) is satisfied at time t_3 when $V_{i,c}$ is smaller than the threshold value $V_{\min}$ and $V_{i,c}$ is continuously decreasing, i.e., $\frac{dV_{i,c}(t_n)}{dt} < \frac{dV_{i,c}(t_{n-5})}{dt}$ for five times t_n which are five time steps apart with the last one being at time t_3 [see Fig. 2(a)]. In the current study, we set $V_{\min}$ equal to $3/15$ which is equal to 0.2 a.u. We find that our results remain almost the same for a range of values of $V_{\min}$. Also, at the end of the laser pulse, we check whether a quasifree electron has positive or negative compensated energy [51]. If the latter occurs, we consider the electron to be bound. Accounting for the effective Coulomb

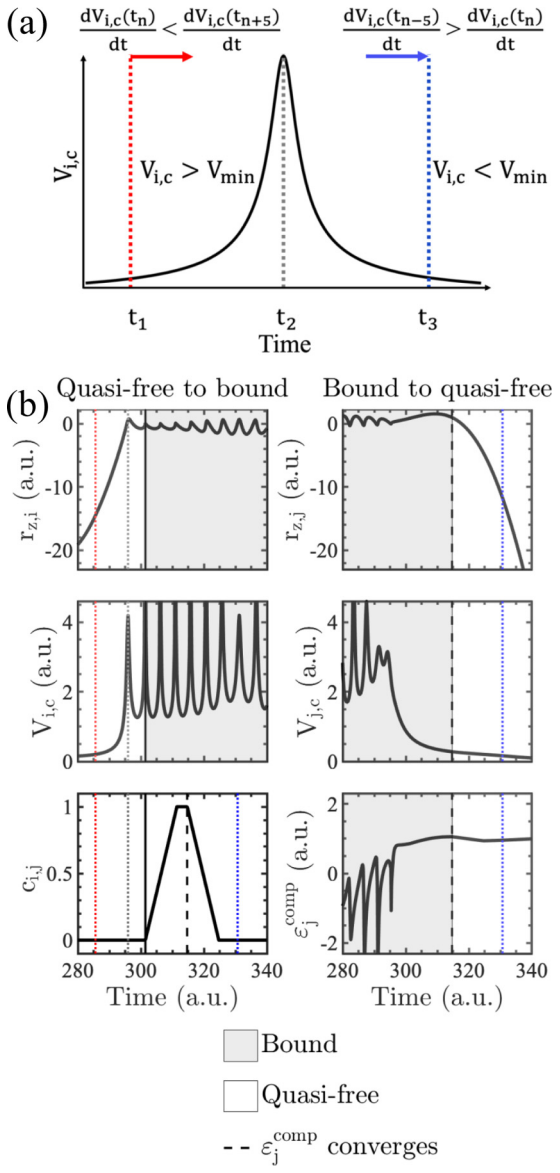

FIG. 2. Schematic illustration of the criteria to determine when a quasifree electron becomes bound (left column) and when a bound electron becomes quasifree (right column).

potential, the compensated energy of electron i is given by

$$\varepsilon_i^{\text{comp}}(t) = \frac{\tilde{\mathbf{p}}_i^2}{2m_i} + \frac{Q_1 Q_i}{|\mathbf{r}_1 - \mathbf{r}_i|} + \sum_{\substack{j=2 \\ j\neq i}}^{N} c_{i,j}(t) V_{\text{eff}}(\zeta_j, |\mathbf{r}_1 - \mathbf{r}_i|). \tag{35}$$

A bound electron transitions to quasifree at time $t > t_0$ if either one of the following two conditions is satisfied: (i) at time t the compensated energy of electron i converges to a positive value or (ii) at times $t = t_3$, $V_{i,c}$ is smaller than the threshold value V_{min} and $V_{i,c}$ is continuously decreasing, i.e., $\frac{dV_{i,c}(t_n)}{dt} < \frac{dV_{i,c}(t_{n-5})}{dt}$ for five t_n which are five time steps apart, the last one being at t_3. The time t when either condition (i) or (ii) is satisfied is a switch time $t_s^{i,j}$ if there is an electron j which is bound (see black solid line in the plot of $c_{i,j}$ as a function of time in Fig. 2). That is, the full Coulomb force between electrons i and j starts to be switched on and the effective potentials start to be switched off.

We illustrate the above criteria in Fig. 2(b). We denote the times t_1, t_2, and t_3 with red, grey, and blue vertical dashed lines, respectively. In the left column, we plot the position r_z and the potential $V_{i,c}$ of a quasifree electron as it transitions to bound. The time when electron i transitions from quasifree to bound because a second extremum is found in the position of electron i along the electric field past the time t_2 is indicated by a vertical black solid line. In the right column, we plot the position r_z, the potential $V_{i,c}$, and the compensated energy of a bound electron as it transitions to quasifree. The time when electron j transitions from bound to quasifree due to the convergence of the compensated energy is indicated by a vertical black dashed line. Moreover, in the left column we plot the coefficient $c_{i,j}$ as a function of time, with the switch times $t_s^{i,j}$ denoted by the vertical black solid and dashed lines. For this specific trajectory, the compensated energy converges prior to t_3 and hence electron i transitions from bound to quasifree at $t < t_3$.

We note that the criteria for the convergence of the compensated energy and the number of extrema in the position of the electron along the laser field have been used to determine whether an electron is quasifree or bound in our previous work on strongly driven three-electron triatomic molecules [33]. However, the criteria presented above are considerably refined compared to the ones in Ref. [33], allowing for the full Coulomb forces to be turned on for a longer time interval. Moreover, in the ECBB model we account for the interaction between bound electrons with effective Coulomb potentials, while in Ref. [33] this interaction was set equal to zero.

D. Initial conditions

1. *Tunnel-ionizing electron*

In both methods, electron 2 tunnel ionizes at time t_0 through the field-lowered Coulomb barrier with a rate that is described by the quantum-mechanical Ammosov-Delone-Krainov (ADK) formula [52,53]. To obtain the ADK rate, we use the value of the energy needed to ionize one electron from Ar; i.e., we use $\text{Ip}_1 = 0.579$ a.u. We find t_0, using importance sampling [54] in the time interval $[-2\tau, 2\tau]$ where the electric field is nonzero; τ is the full width at half maximum of the pulse duration in intensity. The importance sampling distribution is given by the ADK ionization rate. The exit point of electron 2 is along the direction of the laser field and is computed using parabolic coordinates [55]. The momentum of electron 2 is taken to be equal to zero along the laser field. The transverse momentum is given by a Gaussian distribution which represents the Gaussian-shaped filter with an intensity-dependent width arising from standard tunneling theory [53,56,57].

2. *Position and momentum distributions of the bound electrons in the H model*

In the Heisenberg potential, see Eq. (12), for a given α, we find the value of ξ that ensures that the minimum of the

one-electron Hamiltonian,

$$H_i = \frac{\mathbf{p}_i^2}{2m_i} + \frac{Q_1 Q_i}{|\mathbf{r}_1 - \mathbf{r}_i|} + \frac{\xi^2}{4\alpha\mu r_{i,1}^2} \exp\left\{\alpha\left[1 - \left(\frac{r_{i,1}p_{i,1}}{\xi}\right)^4\right]\right\}, \tag{36}$$

corresponds to the third ionization potential of Ar ($\mathrm{Ip}_3 = 1.497$ a.u.) [58–60]. To minimize Eq. (36) with respect to the relative distance $r_{i,1}$, we start from the lower limit of the constraint

$$r_{i,1}p_{i,1} = \xi \Rightarrow p_{i,1} = \xi/r_{i,1}. \tag{37}$$

Since the mass of the core $m_1 \gg m_i$ it follows that $p_{i,1} \approx p_i$. Hence, Eq. (37) can be written as $p_i = \xi/r_{i,1}$ and substituting in Eq. (36) we obtain

$$H_i = \frac{\xi^2}{2m_i r_{i,1}^2} + \frac{Q_1 Q_i}{r_{i,1}} + \frac{\xi^2}{4\alpha\mu r_{i,1}^2}. \tag{38}$$

The minimum of Eq. (38) with respect to $r_{i,1}$ occurs at

$$r_{i,1}^{\min} = -\frac{2\alpha\mu + m_i}{2\alpha\mu m_i Q_1 Q_i}\xi^2, \tag{39}$$

and the energy is given by

$$H_i^{\min} = -\frac{\alpha\mu m_i (Q_1 Q_i)^2}{(m_1 + 2\alpha\mu)\xi^2}. \tag{40}$$

Setting this energy equal to Ip_3, we find $\xi = 1.55$ a.u for $\alpha = 2$ and $\xi = 1.63$ a.u. for $\alpha = 4$. Hence, for $\alpha = 2$ the electrons access a larger phase space during the time propagation.

To find the initial position and momentum vectors of the two initially bound electrons at time t_0, we apply a trial and error method similar to the one proposed by Cohen [31]. First, we randomly sample the magnitude of the position and the momentum vector for each electron in the intervals $[0, r_{\max}]$, $[0, p_{\max}]$. We find that it is sufficient to consider $r_{\max} = 3$ a.u. and $p_{\max} = 3$ a.u. The θ, ϕ polar and azimuthal angles of the position and the momentum of electrons 3 and 4 are obtained as uniform random numbers of $\cos\theta$ in the interval $[-1, 1]$ and ϕ in the interval $[0, 2\pi]$. Using the position and momenta of electrons 3 and 4, we determine the total energy of the two electrons in the absence of the electric field:

$$H_{3,4} = \sum_{i=3}^{4} \frac{\mathbf{p}_i^2}{2} + \sum_{i=3}^{4} \frac{Q_1 Q_i}{|\mathbf{r}_1 - \mathbf{r}_i|} + \sum_{i=3}^{4} V_{H,i} + \frac{Q_3 Q_4}{|\mathbf{r}_3 - \mathbf{r}_4|}. \tag{41}$$

If the energy $H_{3,4}$ is within 1% of the binding energy $\mathrm{Ip}_2 + \mathrm{Ip}_3$, we accept the initial conditions of electrons 3 and 4; otherwise we reject them. For Ar, the energy to ionize a second electron is $\mathrm{Ip}_2 = 1.015$ a.u. Using the above procedure, we plot in Fig. 3 the probability distribution of the initial position and momentum of electrons 3 and 4 as well as of the Heisenberg potential.

3. Position and momentum distributions of the bound electrons in the ECBB model

In the ECBB model, we obtain the initial position and momentum of electron 4 at time t_0 using a microcanonical distribution with an energy

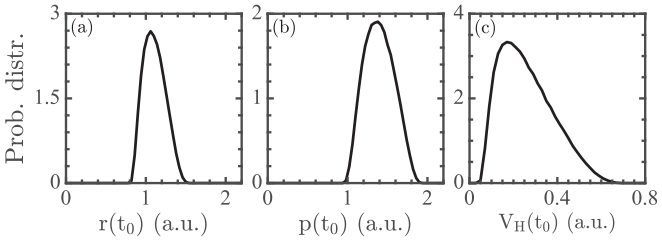

FIG. 3. Probability distribution of (a) r and (b) p for each of electrons 3 and 4 as well as (c) the Heisenberg potential V_H at time t_0, for $\alpha = 2$.

$$\mathcal{E}_4(t_0) = \frac{\mathbf{p}_4^2}{2m_4} + \frac{Q_1 Q_4}{|\mathbf{r}_1 - \mathbf{r}_4|} + V_{\mathrm{eff}}(\zeta_3, |\mathbf{r}_1 - \mathbf{r}_4|), \tag{42}$$

and similarly for electron 3. We take the energy $\mathcal{E}_3(t_0) = \mathcal{E}_4(t_0) = -\mathrm{Ip}_2$ and using Eq. (21) we find that $\zeta_3(t_0) = \zeta_4(t_0) = -(Q_1/\mathcal{E}_{1s})\mathcal{E}_3(t_0)$. The reason we set the initial energy of each electron equal to $-\mathrm{Ip}_2$ is that $\mathcal{E}_4(t_0)$ and $\mathcal{E}_3(t_0)$ include the interaction with the other electron via V_{eff}. Hence, $\mathcal{E}_3(t_0)$ and $\mathcal{E}_4(t_0)$ correspond to the energy needed to remove an electron from Ar^+. Using the above-defined microcanonical distribution, we obtain the initial position and momentum of each bound electron [61]. In Fig. 4, we plot the probability distribution for the initial position and momentum of electrons 3 and 4 as well as of the V_{eff}.

III. RESULTS

In what follows, we compare observables for triple ionization (TI) and double ionization (DI) obtained with the ECBB model and the H model. If available, we also compare these observables with experimental results [21,22]. In our formulation both the ECBB model and the H model fully account for nondipole effects and treat the motion of the electrons and the core on an equal footing.

Here, we employ a vector potential of the form

$$\mathbf{A}(y,t) = -\frac{E_0}{\omega}\exp\left[-2\ln(2)\left(\frac{ct - y}{c\tau}\right)^2\right]\sin(\omega t - ky)\hat{\mathbf{z}}, \tag{43}$$

where $k = \omega/c$ is the wave number of the laser field and τ is the full width at half maximum of the pulse duration in intensity. The direction of both the vector potential and the electric field is along the z axis. We take the propagation direction of

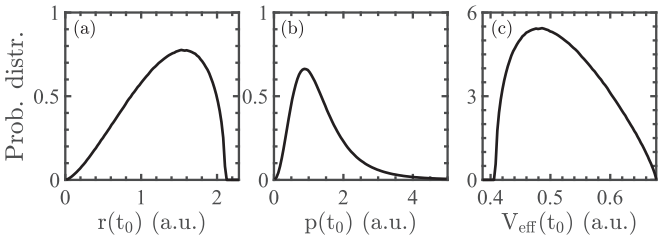

FIG. 4. Probability distribution of (a) r and (b) p for each of electrons 3 and 4 as well as (c) the effective Coulomb potential V_{eff} at time t_0.

the laser field to be along the y axis and hence the magnetic field points along the x axis. We study Ar driven by a laser pulse with intensities ranging from 2×10^{14} to 5×10^{14} W/cm^2 and durations of $\tau = 20$, 25, and 30 fs at 800 nm.

The time propagation of strongly driven Ar starts at time t_0 and stops at an asymptotically large time t_f. For each trajectory, if the energies of three (two) electrons are positive, we label the trajectory as a triple (double) ionization event. The DI and TI probabilities are

$$P_{\rm DI} = \frac{N_{\rm DI}}{N}, \quad P_{\rm TI} = \frac{N_{\rm TI}}{N}, \tag{44}$$

where $N_{\rm DI}$, $N_{\rm TI}$, and N are the numbers of doubly ionized, triply ionized, and all events, respectively. Here, we mainly focus on nonsequential double ionization (NSDI) and on nonsequential triple ionization (NSTI) events. NSDI and NSTI involve an electron accelerating in the laser field and coming back to the core to transfer energy to bound electrons via a recollision. This energy transfer can lead to the escape of two electrons (NSDI) or three electrons (NSTI). Electronic correlation, a fundamental interaction, underlies this field-assisted recollision [62].

To identify a recollision in either one of the two models, we monitor the Coulomb potential between all pairs of a quasifree and a bound electron. We identify the maxima in the interelectronic Coulomb potential energy as function of time. We label the times when the interelectronic distance is a minimum as recollision times $t_{\rm rec}$. Also, we define the ionization time of electron i, $t^i_{\rm ion}$, to be the time when the compensated energy becomes positive and remains positive thereafter [51]. We used the same definition for $t^i_{\rm ion}$ in all our previous studies (see for instance Refs. [7,63]). The compensated energy is given by

$$\varepsilon_i^{\rm comp}(t) = \frac{\tilde{\mathbf{p}}_i^2}{2m_i} + \frac{Q_1 Q_i}{|\mathbf{r}_1 - \mathbf{r}_i|} + \sum_{\substack{j=2 \\ j\neq i}}^{N} c_{i,j}(t) V_{\rm eff}(\zeta_j, |\mathbf{r}_1 - \mathbf{r}_i|),$$

$$\varepsilon_i^{\rm comp}(t) = \frac{\tilde{\mathbf{p}}_i^2}{2m_i} + \frac{Q_1 Q_i}{|\mathbf{r}_1 - \mathbf{r}_i|} + V_{H,i},$$

for the ECBB and the H model, respectively. Moreover, a TI or DI event is labeled as direct if the energy transferred from a recolliding electron to bound electrons suffices for the simultaneous ionization, shortly after recollision, of three or two electrons. In Appendix C, we outline the algorithm used to label an event as direct. Here, we label the remaining events as delayed TI and DI events.

A. DI and TI probabilities

We find that the DI and TI probabilities are consistently larger for the H model for both $\alpha = 2, 4$ compared to the ECBB model. This is consistent with the different initial conditions the bound electrons have in the two models. The initial momenta of the bound electrons are higher in the H model versus the ECBB model [compare Fig. 3(b) with Fig. 4(b)]. Also, the repulsive Heisenberg potential reduces the attraction of each electron from the core resulting in higher ionization probabilities. Regarding the DI probability, for the H model, we find that at intensities 2×10^{14}, 4×10^{14}, and 5×10^{14} W/cm^2 and 20 fs pulse duration the DI probability is consistently higher for $\alpha = 4$ compared to $\alpha = 2$. However, while at the two smallest intensities the difference in the DI probability is small for the two values of α, at 5×10^{14} W/cm^2 the DI probability is almost 71% higher for $\alpha = 4$ compared to $\alpha = 2$. Hence, the DI probability depends significantly on the value of α, a disadvantage of the H model. In what follows, we consider $\alpha = 2$ for the H model, unless otherwise stated, since this value allows the electrons to access a larger phase space. As we increase the intensity from 2×10^{14} to 5×10^{14} W/cm^2, we find that the ratio of the DI probabilities between the two models, $P_{\rm DI}^{\rm ECBB}/P_{\rm DI}^{\rm H}$, decreases from 1.1 to 0.4. However, the ratio of the TI probabilities $P_{\rm TI}^{\rm ECBB}/P_{\rm TI}^{\rm H}$ increases from 0.03 to 0.2. Hence, for the intensities considered here, the DI and TI probabilities are smaller for the ECBB model.

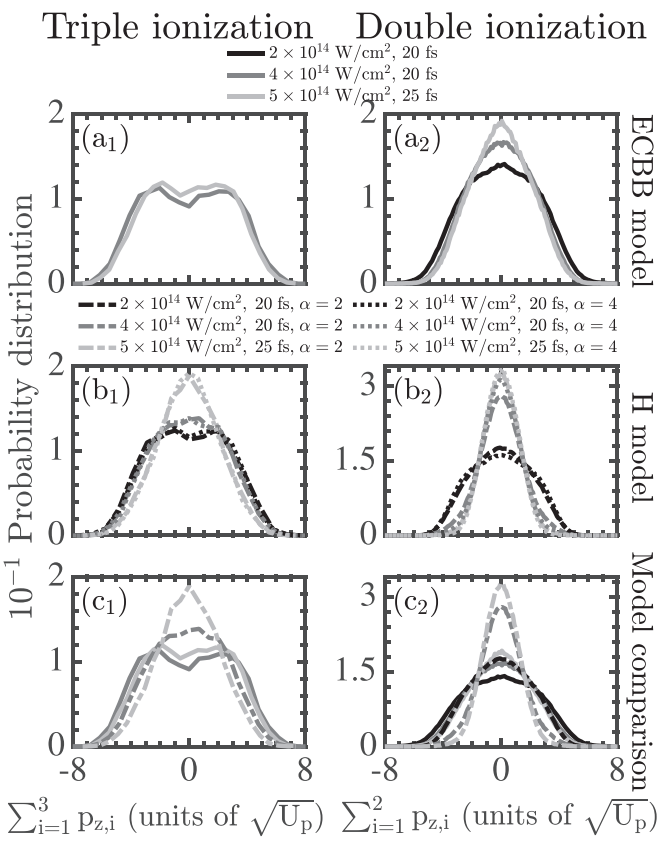

FIG. 5. Probability distributions of the sum of the electron momentum components parallel to the polarization of the laser field for TI (left column) and DI (right column) at intensities 2×10^{14} W/cm^2 (20 fs), 4×10^{14} W/cm^2 (20 fs), and 5×10^{14} W/cm^2 (25 fs). The ECBB model results are presented in the top row, the H model results in the middle row, and a comparison of the two models in the third row. All probability distributions are normalized to one.

B. Distribution of the sum of the electron momenta

In Fig. 5, we plot the TI and DI probability distribution of the sum of the p_z momenta of the ionizing electrons at intensities 2×10^{14} and 4×10^{14} W/cm^2 and 20 fs pulse duration and 5×10^{14} W/cm^2 and 25 fs pulse duration. The highest intensity pulse allows for a direct comparison with experimental results [19]. In Figs. 5(a1) and 5(a2), for the ECBB model, we plot the TI and DI probability distributions of the sum of the p_z

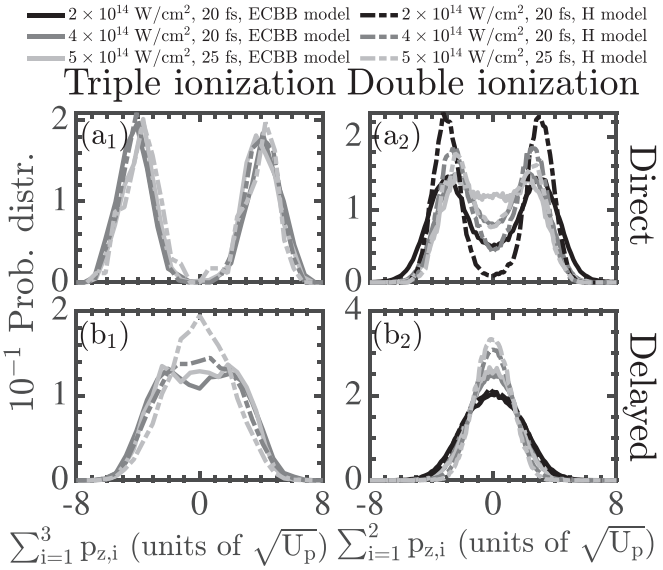

FIG. 6. Probability distributions of the sum of electron momenta components parallel to the polarization of the laser field for TI (left column) and DI (right column) at intensities 2×10^{14} W/cm^2 (20 fs), 4×10^{14} W/cm^2 (20 fs), and 5×10^{14} W/cm^2 (25 fs). The direct pathway distributions are plotted on the top row and the delayed pathway distributions are plotted on the bottom row. All probability distributions are normalized to one.

momenta of the ionizing electrons. For DI [Fig. 5(a2)], we find that the probability distribution is centered around zero and the width decreases with increasing intensity. This is in accord with our previous findings for two-electron Ar driven by a 4 fs pulse for intensities from 2×10^{14} to 5×10^{14} W/cm^2 [35]. For TI [Fig. 5(a1)], we find similar doubly peaked distributions for 4×10^{14} and 5×10^{14} W/cm^2. The TI probability at 2×10^{14} W/cm^2 is very low and we do not consider this intensity in Fig. 5(a1).

In Figs. 5(b1) and 5(b2), for the H model for $\alpha = 2, 4$, we plot the TI and DI probability distributions of the sum of the p_z momenta of the ionizing electrons. For DI [Fig. 5(b2)], we find that the probability distribution is centered around zero and the width decreases with increasing intensity for both α. For TI [Fig. 5(b1)], we find that at 2×10^{14} W/cm^2 the distribution is doubly peaked, while at higher intensities the distribution is centered around zero. Finally, we find that the TI distributions are similar for the two values of α, while the DI distributions are more centered around zero for $\alpha = 4$. This is consistent with each electron being less attracted from the core for larger values of α resulting in smaller final momenta. Hence, the probability distributions depend on the value of α.

Comparing the TI [Fig. 5(c1)] and DI [Fig. 5(c2)] probability distributions of the ECBB and H models for $\alpha = 2$, we find that all distributions are more centered around zero for the H model. Moreover, the TI distributions at higher intensities are doubly peaked for the ECBB model and centered around zero for the H model.

In Fig. 6, we plot the TI and DI distributions of the sum of the p_z electron momenta for the direct (top row) and delayed pathway (bottom row). In the delayed pathway, we account

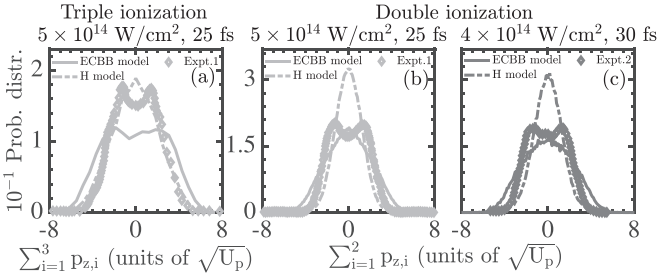

FIG. 7. Probability distributions of the sum of electron momenta components parallel to the polarization of the laser field for (a) TI and (b, c) DI at intensities 5×10^{14} W/cm^2 (25 fs) in (a) and (b) and 4×10^{14} W/cm^2 (30 fs) in (c). We compare the distributions obtained with the ECBB and H models with experimental ones [21,22]. All probability distributions are normalized to one.

for all nondirect events. Hence, here, the delayed events also include TI and DI no-recollision events. The latter account for roughly 7% of DI and 4% of TI events for the H model and zero for the ECBB model.

For the direct pathway, we find that the TI [Fig. 6(a1)] and DI [Fig. 6(a2)] distributions are double peaked for both the ECBB and the H model. For TI events the distributions have peaks at larger values of momenta compared to DI events, with the peaks for TI being around $\pm4\sqrt{U_p}$ and for DI around $\pm2.5\sqrt{U_p}$. The ponderomotive energy $U_p = E_0^2/(4\omega^2)$ is the average energy an electron gains from the laser field. Also, for DI events, the distributions have more events centered around zero for the ECBB compared to the H model. This contribution increases with increasing intensity, which is consistent with our previous results of double ionization of two-electron Ar driven by short pulses [35]. We find the percentage of direct events to be significantly larger for the ECBB compared to the H model. The contribution of direct events to DI is roughly 50% for the ECBB model, while it decreases from 16% to 5% with increasing intensity for the H model. The contribution of direct events to TI is roughly 20% for the ECBB model while it is roughly 5% for the H model at the two highest intensities. For the delayed pathway, for DI, the distributions are centered around zero for both models [Fig. 6(b2)], while for TI the distributions are less centered around zero for the ECBB model [Fig. 6(b1)].

Next, we compare with experimental results the findings of the ECBB and H models for the DI distribution of the sum of the p_z electron momenta of Ar at 4×10^{14} W/cm^2 (30 fs) [Fig. 7(c)] and 5×10^{14} W/cm^2 (25 fs) [Fig. 7(b)] [21,22] as well as the TI distribution at 5×10^{14} W/cm^2 (25 fs) [22] [Fig. 7(a)]. The experimental DI distributions have a slight double-peaked structure and agree more with the results of the ECBB model. Indeed, the H model produces DI distributions that are highly centered around zero, which is significantly less the case for the ECBB model. The experimental TI distributions have a slight doubly peaked structure which is only reproduced by the ECBB model. However, the TI distribution obtained with the ECBB model is wider than the one obtained experimentally. Hence, for DI the ECBB model better reproduces the experimental results while for TI it is not clear whether the ECBB or the H model agrees best

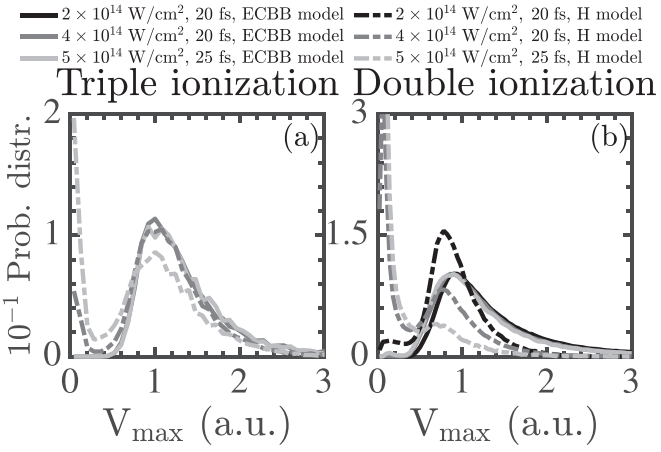

FIG. 8. Probability distributions of the largest value of the Coulomb interelectronic potential energy for (a) TI and (b) DI at intensities 2×10^{14} W/cm^2 (20 fs), 4×10^{14} W/cm^2 (20 fs), and 5×10^{14} W/cm^2 (25 fs). All probability distributions are normalized to one.

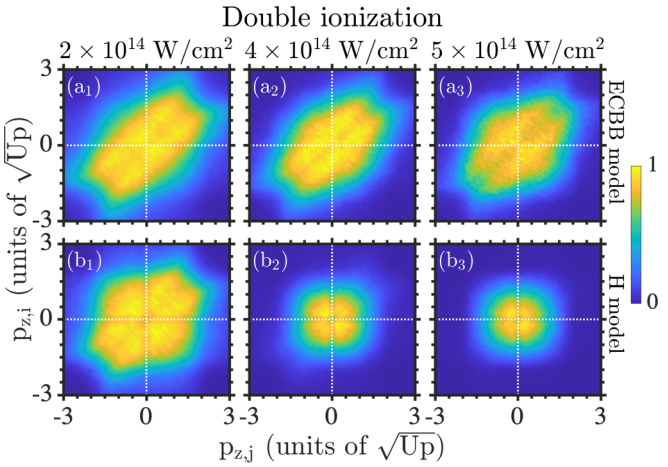

FIG. 9. Symmetrized correlated momenta of all pairs of escaping electrons for DI for (a1–a3) the ECBB model and (b1–b3) the H model at intensities 2×10^{14} W/cm^2 (20 fs), 4×10^{14} W/cm^2 (20 fs), and 5×10^{14} W/cm^2 (25 fs). The doubly differential distributions are divided by the peak value.

with experiment. To answer this question a future study needs to compare distributions where intensity averaging has been accounted for in the theoretical results [35,64].

C. Strength of the recollision in DI and TI events

For each DI and TI event we register all the maxima of the Coulomb interelectronic potential energy as a function of time and identify the largest maximum $V_{\max}$. That is, we identify the most important recollision for each event. We plot the distribution of $V_{\max}$ for TI [Fig. 8(a)] and DI [Fig. 8(b)] events. We find that recollisions are significantly stronger for the ECBB model, with the most probable value of $V_{\max}$ being roughly 1 a.u. for DI and TI at all intensities. In contrast, for the H model, at the higher intensities, the most probable value of $V_{\max}$ is close to 0 a.u. both for DI and TI. For the H model, weaker recollisions are consistent with the DI and TI distributions of the sum of the p_z electron momenta being more centered around zero (see Fig. 5).

D. Correlated momenta

In Fig. 9, for DI, we plot the correlated electron momenta at intensities 2×10^{14} W/cm^2 (20 fs), 4×10^{14} W/cm^2 (20 fs), and 5×10^{14} W/cm^2 (25 fs) obtained with the ECBB model [Figs. 9(a1)–9(a3)] and the H model [Figs. 9(b1)–9(b3)]. At the three intensities, we find that correlated electron escape prevails mostly for the ECBB model which produces roughly 10% more correlated events than the H model. Also, at intensities 4×10^{14} and 5×10^{14} W/cm^2, the electrons escape with considerably higher momenta in the ECBB model [compare Fig. 9(a2) with Fig. 9(b2) and Fig. 9(a3) with Fig. 9(b3)]. The above are consistent with the ECBB model resulting in more direct events (Sec. III B) and stronger recollisions (Fig. 8) than the H model.

In Fig. 10, for TI, we plot the correlated electron momenta at intensities 4×10^{14} W/cm^2 (20 fs) and 5×10^{14} W/cm^2 (25 fs) obtained with the ECBB model [Figs. 10(a1) and 10(a2)] and the H model [Figs. 10(b1) and 10(b2)]. We find that correlated three-electron escape is clearly prevalent at both intensities for the ECBB model, while this is barely the case for the H model. Moreover, the three electrons escape with significantly smaller momenta for the H model compared to the ECBB model [compare Fig. 10(a1) with Fig. 10(b1) and Fig. 10(a2) with Fig. 10(b2). As for DI, this is consistent with the ECBB model yielding more direct events and stronger recollisions versus the H model.

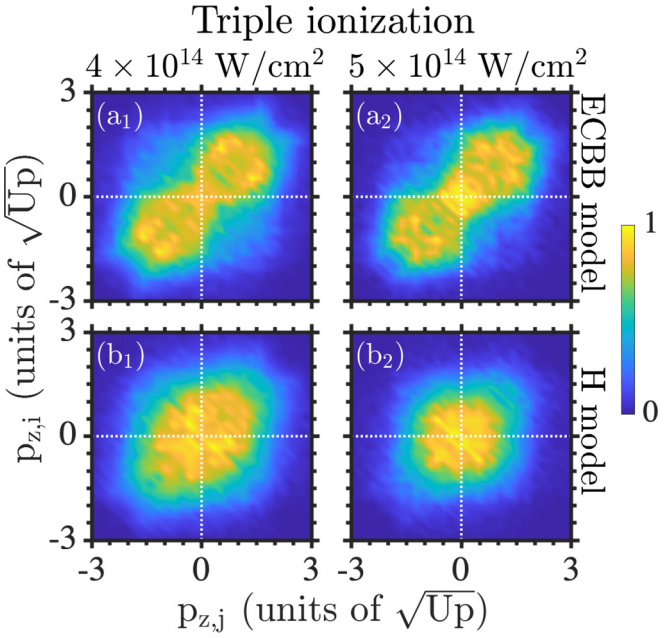

FIG. 10. Symmetrized correlated momenta of all pairs of escaping electrons for TI for (a1, a2) the ECBB model and (b1, b2) the H model at intensities 4×10^{14} W/cm^2 (20 fs) and 5×10^{14} W/cm^2 (25 fs). The doubly differential distributions are divided by the peak value.

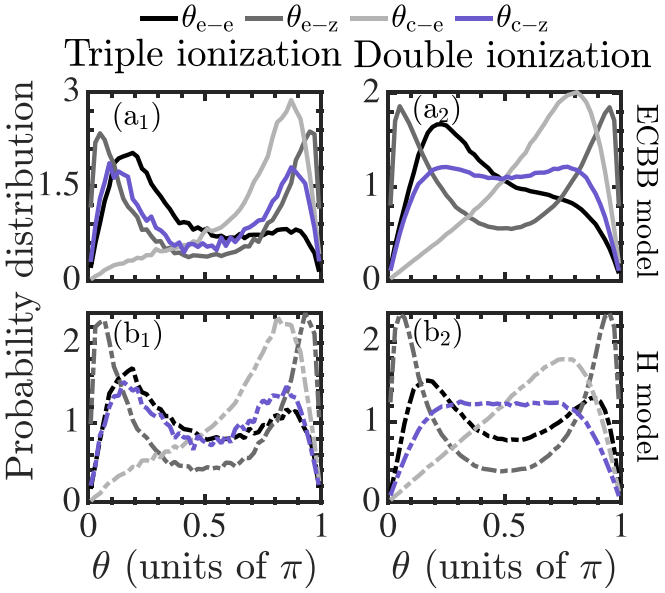

FIG. 11. Probability distributions of the angles of the ionizing electrons and the core for TI (left column) and DI (right column) at 4×10^{14} W/cm^2 (20 fs). Plots for the ECBB model are denoted with solid lines versus broken lines for the H model. All probability distributions are normalized to one.

E. Angular distributions

In Fig. 11, we plot the TI (left column) and DI (right column) probability distributions of the angles of the ionizing electrons and the core at intensity 4×10^{14} W/cm^2 at 20 fs. We obtain similar results for the other intensities considered in this work (not shown). We find that the angle between any pair of escaping electrons θ_{e-e} (black color) is mostly peaked at small angles, indicating a correlated electron escape. For both the ECBB model and the H model, we find that the angle of interelectronic escape is smaller for TI versus DI. This is consistent with the electron momenta being more correlated for TI versus DI (compare Fig. 9 with Fig. 10). We also find that a small angle of interelectronic escape is significantly more favored by the ECBB model, which results in more direct events and stronger recollisions.

We also find that the angle of any escaping electron with the z axis, θ_{e-z} (dark gray color), peaks at small and large values for TI and DI for both models. That is, the ionizing electrons escape mostly along (0°) or opposite (180°) the direction of the electric field. However, the peaks of the distributions of θ_{e-z} are sharper, i.e., the distributions are less wide, for the H model. This is in accord with our finding that the H model gives rise to a significantly higher number of TI and DI events where no recollision takes place compared to the ECBB model. As a result, in the H model, the electrons ionize mostly due to the field for a larger number of events, with the electrons escaping more along or opposite the direction of the field. Moreover, we find that the distributions of the angle of the core with the z axis, θ_{c-z} (blue color), are wide for both TI and DI for both models. However, the distribution is wider for DI versus TI. This is consistent with the core having a higher charge equal to 3 for TI versus 2 for DI. As a result, the electric field exerts a larger force on the core in TI leading the core to escape more along or opposite the direction of the electric field. Finally, we find that the distribution of the angle θ_{c-e} (light grey color) between an ionizing electron and the core peaks mostly at large angles; that is, the electron and the core escape in opposite directions. This is consistent with the electric field exerting opposite forces to particles of opposite charges. We find that the angle of escape between an electron and the core is larger for TI compared to DI for both models. This is consistent with the larger core charge for TI resulting in the core escaping more along or opposite the field direction.

IV. CONCLUSIONS

We formulate a 3D semiclassical model to address three-electron dynamics in a strongly driven atom where the electron and core dynamics are treated at the same time. Our formulation includes the magnetic field of the laser field as well as the Coulomb singularities. We address unphysical autoionization present in semiclassical models where the Coulomb singularities are accounted for and more than one electron is bound. We do so by substituting the Coulomb repulsion between bound electrons with effective potentials where an effective charge is associated with every bound electron. The interaction between pairs of electrons that are not both bound is accounted for with the full Coulomb potential and all other forces are fully accounted for. This model, developed in this work and referred to as the ECBB model, identifies on the fly during time propagation if an electron is bound or not. We compare the ionization spectra obtained with the ECBB model with the ones obtained with a model previously developed—referred to here as the H model. In the latter model, a potential is added for each electron that mimics the Heisenberg uncertainty principle and restricts the accessible phase space of each electron preventing autoionization. The advantage of the ECBB model is that it accurately treats the interaction of each electron with the core and all other interactions while it treats less accurately the interaction between bound electrons. The advantage of the H model is that it accurately treats the interaction between all electrons while it treats less accurately the interaction of each electron with the core.

Using these 3D semiclassical models, we address triple and double ionization in a strongly driven atom, namely, Ar. We compare the ionization spectra obtained with the two models as well as with experiment for various pulse durations and intensities. We find that both double- and triple-ionization probabilities are greater for the H model compared to the ECBB model. We conjecture that this difference in the probabilities is due to the Heisenberg potential resulting in larger initial momenta of the bound electrons as well as in significant less attraction of each electron from the core. We find that in the H model for a significant number of events the electrons ionize without a recollision, i.e., ionize due to the laser field, and the recollisions are significantly weaker compared to the ECBB model. These findings are consistent with our results for the distribution of the sum of the momenta of the ionizing electrons along the direction of the laser field. For all the intensities and pulse durations considered here, we find that

these distributions are broader for the ECBB model. For triple ionization, we find that the distributions of the sum of the electron momenta have a double peak for the ECBB model while they are centered around zero for the H model. We find this to be due to the ECBB model producing more direct-ionization events than the H model. This is also evident in the correlated electron momenta where the distributions obtained with the ECBB model are consistently more correlated compared to the ones obtained with the H model. Moreover, we identify another disadvantage of the H model; namely, the distributions of the momenta and ionization probabilities depend on the parameter α in the Heisenberg potential. Comparing with experimental distributions of the sum of the momenta we find that the distributions obtained with the ECBB model have a better agreement with experiment mainly for double ionization. Finally, our formulation of the ECBB model and of the H model that accounts for electron and core motion and for nondipole effects is general and can be generalized to strongly driven atoms with more than three electrons.

ACKNOWLEDGMENTS

A.E. and G.P.K. acknowledge the EPSRC Grant No. EP/W005352/1. The authors acknowledge the use of the UCL Myriad High Throughput Computing Facility (Myriad@UCL), and associated support services, in the completion of this work. Moreover, the authors are grateful to Professor Armin Scrinzi for useful discussions.

APPENDIX A: DERIVATION OF THE EFFECTIVE POTENTIAL

The electric field produced by a charge $Q(\zeta_j, r)$ that is contained within a spherical shell of radius r from the core is obtained by Gauss's law as follows:

$$\mathbf{E}(\zeta_j, r) = \frac{Q(\zeta_j, r)}{r^2}\hat{r}. \tag{A1}$$

The work W done on a particle i due to the electric field $\mathbf{E}(\zeta_j, r)$ is equal to minus the change in potential energy ΔV_{eff}:

$$\begin{aligned} W &= -\Delta V_{\text{eff}} \\ &= -[V_{\text{eff}}(\zeta_j, r) - V_{\text{eff}}(\zeta_j, \infty)] \\ &= -V_{\text{eff}}(\zeta_j, r), \end{aligned} \tag{A2}$$

where we have used that $V_{\text{eff}}(\zeta_j, \infty) = 0$. The work W is also given by

$$\begin{aligned} W &= \int_\infty^r \mathbf{F}\cdot d\mathbf{r}' = -\int_\infty^r \mathbf{E}\cdot d\mathbf{r}' \\ &= -\int_\infty^r E(\zeta_j, r')(\hat{r}'\cdot\hat{r}')dr' \\ &= \int_\infty^r \left[\frac{1}{r'^2} - \frac{e^{-2\zeta_j r'}(1+2\zeta_j r')}{r'^2} - 2\zeta_j^2 e^{-2\zeta_j r'}\right]dr' \\ &= \left(-\frac{1}{r'} + \frac{e^{-2\zeta_j r'}}{r'} + \zeta_j e^{-2\zeta_j r'}\right)\Big|_\infty^r \\ &= -\frac{1-(1+\zeta_j r)e^{-2\zeta_j r}}{r}, \end{aligned} \tag{A3}$$

where we have used that particle i is an electron and hence $\mathbf{F} = -\mathbf{E}$ as well as that particle j is an electron and $Q(\zeta_j, r)$ is given by Eq. (19). Using Eqs. (A2) and (A3), we find

$$V_{\text{eff}}(\zeta_j, r) = \frac{1-(1+\zeta_j r)e^{-2\zeta_j r}}{r}, \tag{A4}$$

which is the potential energy that an electron i has at a distance r from the core due to a bound electron j.

APPENDIX B: LEAPFROG ALGORITHM

In what follows, we describe the leapfrog algorithm. First, we initialize the auxiliary variables $\mathbf{W}_0^{\mathbf{q}} = \mathbf{q}_0$, $\mathbf{W}_0^{\boldsymbol{\rho}} = \boldsymbol{\rho}_0$, $W_0^t = t_0$, and $W_0^{\mathcal{E}} = \mathcal{E}_0$. Then, we propagate for a time step equal to h, by propagating for half a step each quadruplet of variables $(\mathbf{q}, \mathbf{W}^{\boldsymbol{\rho}}, t, W^{\mathcal{E}})$ and $(\mathbf{W}^{\mathbf{q}}, \boldsymbol{\rho}, W^t, \mathcal{E})$ in an alternating way as follows:

$$\begin{aligned}
\mathbf{q}_{1/2} &= \mathbf{q}_0 + \frac{h}{2}\frac{\dot{\mathbf{q}}\left(\mathbf{W}_0^{\mathbf{q}}, \boldsymbol{\rho}_0, W_0^t\right)}{\Omega\left(\mathbf{W}_0^{\mathbf{q}}\right)}, \\
\mathbf{W}_{1/2}^{\boldsymbol{\rho}} &= \mathbf{W}_0^{\boldsymbol{\rho}} + \frac{h}{2}\frac{\dot{\boldsymbol{\rho}}\left(\mathbf{W}_0^{\mathbf{q}}, \boldsymbol{\rho}_0, W_0^t, \mathcal{E}_0\right)}{\Omega\left(\mathbf{W}_0^{\mathbf{q}}\right)}, \\
t_{1/2} &= t_0 + \frac{h}{2}\frac{1}{\Omega\left(\mathbf{W}_0^{\mathbf{q}}\right)}, \\
W_{1/2}^{\mathcal{E}} &= W_0^{\mathcal{E}} + \frac{h}{2}\frac{\dot{\mathcal{E}}\left(\mathbf{W}_0^{\mathbf{q}}, \boldsymbol{\rho}_0, W_0^t, \mathcal{E}_0\right)}{\Omega\left(\mathbf{W}_0^{\mathbf{q}}\right)}, \\
\mathbf{W}_1^{\mathbf{q}} &= \mathbf{W}_0^{\mathbf{q}} + h\frac{\dot{\mathbf{q}}(\mathbf{q}_{1/2}, \mathbf{W}_{1/2}^{\boldsymbol{\rho}}, t_{1/2})}{\Omega(\mathbf{q}_{1/2})}, \\
\boldsymbol{\rho}_1 &= \boldsymbol{\rho}_0 + h\frac{\dot{\boldsymbol{\rho}}(\mathbf{q}_{1/2}, \mathbf{W}_{1/2}^{\boldsymbol{\rho}}, t_{1/2}, W_{1/2}^{\mathcal{E}})}{\Omega(\mathbf{q}_{1/2})}, \\
W_1^t &= W_0^t + h\frac{1}{\Omega(\mathbf{q}_{1/2})}, \\
\mathcal{E}_1 &= \mathcal{E}_0 + h\frac{\dot{\mathcal{E}}(\mathbf{q}_{1/2}, \mathbf{W}_{1/2}^{\boldsymbol{\rho}}, t_{1/2}, W_{1/2}^{\mathcal{E}})}{\Omega(\mathbf{q}_{1/2})}, \\
\mathbf{q}_1 &= \mathbf{q}_{1/2} + \frac{h}{2}\frac{\dot{\mathbf{q}}\left(\mathbf{W}_1^{\mathbf{q}}, \boldsymbol{\rho}_1, W_1^t\right)}{\Omega\left(\mathbf{W}_1^{\mathbf{q}}\right)}, \\
\mathbf{W}_1^{\boldsymbol{\rho}} &= \mathbf{W}_{1/2}^{\boldsymbol{\rho}} + \frac{h}{2}\frac{\dot{\boldsymbol{\rho}}\left(\mathbf{W}_1^{\mathbf{q}}, \boldsymbol{\rho}_1, W_1^t, \mathcal{E}_1\right)}{\Omega\left(\mathbf{W}_1^{\mathbf{q}}\right)}, \\
t_1 &= t_{1/2} + \frac{h}{2}\frac{1}{\Omega(\mathbf{W}_1^{\mathbf{q}})}, \\
W_1^{\mathcal{E}} &= W_{1/2}^{\mathcal{E}} + \frac{h}{2}\frac{\dot{\mathcal{E}}\left(\mathbf{W}_1^{\mathbf{q}}, \boldsymbol{\rho}_1, W_1^t, \mathcal{E}_1\right)}{\Omega\left(\mathbf{W}_1^{\mathbf{q}}\right)}.
\end{aligned}$$

The subscripts 0, 1/2, and 1 denote the value of each variable at the start, the middle, and the end of the time step h.

Next, we describe the algorithm that incorporates the leapfrog method in the Bulirsch-Stoer extrapolation scheme

over a step H, which is split into n substeps of size $h = H/n$:

$$\mathbf{q}_{1/2} = \mathbf{q}_0 + \frac{h}{2}\frac{\dot{\mathbf{q}}(\mathbf{W}_0^{\mathbf{q}}, \boldsymbol{\rho}_0, W_0^t)}{\Omega(\mathbf{W}_0^{\mathbf{q}})},$$

$$\mathbf{W}_{1/2}^{\boldsymbol{\rho}} = \mathbf{W}_0^{\boldsymbol{\rho}} + \frac{h}{2}\frac{\dot{\boldsymbol{\rho}}(\mathbf{W}_0^{\mathbf{q}}, \boldsymbol{\rho}_0, W_0^t, \mathcal{E}_0)}{\Omega(\mathbf{W}_0^{\mathbf{q}})},$$

$$t_{1/2} = t_0 + \frac{h}{2}\frac{1}{\Omega(\mathbf{W}_0^{\mathbf{q}})},$$

$$W_{1/2}^{\mathcal{E}} = W_0^{\mathcal{E}} + \frac{h}{2}\frac{\dot{\mathcal{E}}(\mathbf{W}_0^{\mathbf{q}}, \boldsymbol{\rho}_0, W_0^t, \mathcal{E}_0)}{\Omega(\mathbf{W}_0^{\mathbf{q}})},$$

$$\mathbf{W}_1^{\mathbf{q}} = \mathbf{W}_0^{\mathbf{q}} + h\frac{\dot{\mathbf{q}}(\mathbf{q}_{1/2}, \mathbf{W}_{1/2}^{\boldsymbol{\rho}}, t_{1/2})}{\Omega(\mathbf{q}_{1/2})},$$

$$\boldsymbol{\rho}_1 = \boldsymbol{\rho}_0 + h\frac{\dot{\boldsymbol{\rho}}(\mathbf{q}_{1/2}, \mathbf{W}_{1/2}^{\boldsymbol{\rho}}, t_{1/2}, W_{1/2}^{\mathcal{E}})}{\Omega(\mathbf{q}_{1/2})},$$

$$W_1^t = W_0^t + h\frac{1}{\Omega(\mathbf{q}_{1/2})},$$

$$\mathcal{E}_1 = \mathcal{E}_0 + h\frac{\dot{\mathcal{E}}(\mathbf{q}_{1/2}, \mathbf{W}_{1/2}^{\boldsymbol{\rho}}, t_{1/2}, W_{1/2}^{\mathcal{E}})}{\Omega(\mathbf{q}_{1/2})},$$

$$\vdots$$

$$\mathbf{q}_{m-1/2} = \mathbf{q}_{m-3/2} + h\frac{\dot{\mathbf{q}}(\mathbf{W}_{m-1}^{\mathbf{q}}, \boldsymbol{\rho}_{m-1}, W_{m-1}^t)}{\Omega(\mathbf{W}_{m-1}^{\mathbf{q}})},$$

$$\mathbf{W}_{m-1/2}^{\boldsymbol{\rho}} = \mathbf{W}_{m-3/2}^{\boldsymbol{\rho}} + h\frac{\dot{\boldsymbol{\rho}}(\mathbf{W}_{m-1}^{\mathbf{q}}, \boldsymbol{\rho}_{m-1}, W_{m-1}^t, \mathcal{E}_{m-1})}{\Omega(\mathbf{W}_{m-1}^{\mathbf{q}})},$$

$$t_{m-1/2} = t_{m-3/2} + h\frac{1}{\Omega(\mathbf{W}_{m-1}^{\mathbf{q}})},$$

$$W_{m-1/2}^{\mathcal{E}} = W_{m-3/2}^{\mathcal{E}} + h\frac{\dot{\mathcal{E}}(\mathbf{W}_{m-1}^{\mathbf{q}}, \boldsymbol{\rho}_{m-1}, W_{m-1}^t, \mathcal{E}_{m-1})}{\Omega(\mathbf{W}_{m-1}^{\mathbf{q}})},$$

$$\mathbf{W}_m^{\mathbf{q}} = \mathbf{W}^{\mathbf{q}}{}_{m-1} + h\frac{\dot{\mathbf{q}}(\mathbf{q}_{m-1/2}, \mathbf{W}_{m-1/2}^{\boldsymbol{\rho}}, t_{m-1/2})}{\Omega(\mathbf{q}_{m-1/2})},$$

$$\boldsymbol{\rho}_m = \boldsymbol{\rho}_{m-1} + h\frac{\dot{\boldsymbol{\rho}}(\mathbf{q}_{m-1/2}, \mathbf{W}_{m-1/2}^{\boldsymbol{\rho}}, t_{m-1/2}, W_{m-1/2}^{\mathcal{E}})}{\Omega(\mathbf{q}_{m-1/2})},$$

$$W_m^t = W_{m-1}^t + h\frac{1}{\Omega(\mathbf{q}_{m-1/2})},$$

$$\mathcal{E}_m = \mathcal{E}_{m-1} + h\frac{\dot{\mathcal{E}}(\mathbf{q}_{m-1/2}, \mathbf{W}_{m-1/2}^{\boldsymbol{\rho}}, t_{m-1/2}, W_{m-1/2}^{\mathcal{E}})}{\Omega(\mathbf{q}_{m-1/2})},$$

$$\vdots$$

$$\mathbf{W}_n^{\mathbf{q}} = \mathbf{W}^{\mathbf{q}}{}_{n-1} + h\frac{\dot{\mathbf{q}}(\mathbf{q}_{n-1/2}, \mathbf{W}_{n-1/2}^{\boldsymbol{\rho}}, t_{n-1/2})}{\Omega(\mathbf{q}_{n-1/2})},$$

$$\boldsymbol{\rho}_n = \boldsymbol{\rho}_{n-1} + h\frac{\dot{\boldsymbol{\rho}}(\mathbf{q}_{n-1/2}, \mathbf{W}_{n-1/2}^{\boldsymbol{\rho}}, t_{n-1/2}, W_{n-1/2}^{\mathcal{E}})}{\Omega(\mathbf{q}_{n-1/2})},$$

$$W_n^t = W_{n-1}^t + h\frac{1}{\Omega(\mathbf{q}_{n-1/2})},$$

$$\mathcal{E}_n = \mathcal{E}_{n-1} + h\frac{\dot{\mathcal{E}}(\mathbf{q}_{n-1/2}, \mathbf{W}_{n-1/2}^{\boldsymbol{\rho}}, t_{n-1/2}, W_{n-1/2}^{\mathcal{E}})}{\Omega(\mathbf{q}_{n-1/2})},$$

$$\mathbf{q}_n = \mathbf{q}_{n-1/2} + \frac{h}{2}\frac{\dot{\mathbf{q}}(\mathbf{W}_n^{\mathbf{q}}, \boldsymbol{\rho}_n, W_n^t)}{\Omega(\mathbf{W}_n^{\mathbf{q}})},$$

$$\mathbf{W}_n^{\boldsymbol{\rho}} = \mathbf{W}_{n-1/2}^{\boldsymbol{\rho}} + \frac{h}{2}\frac{\dot{\boldsymbol{\rho}}(\mathbf{W}_n^{\mathbf{q}}, \boldsymbol{\rho}_n, W_n^t, \mathcal{E}_n)}{\Omega(\mathbf{W}_n^{\mathbf{q}})},$$

$$t_n = t_{n-1/2} + \frac{h}{2}\frac{1}{\Omega(\mathbf{W}_n^{\mathbf{q}})},$$

$$W_n^{\mathcal{E}} = W_{n-1/2}^{\mathcal{E}} + \frac{h}{2}\frac{\dot{\mathcal{E}}(\mathbf{W}_n^{\mathbf{q}}, \boldsymbol{\rho}_n, W_n^t, \mathcal{E}_n)}{\Omega(\mathbf{W}_n^{\mathbf{q}})},$$

where $m = 2, \ldots, n-1$.

APPENDIX C: IDENTIFYING THE DIRECT PATHWAY OF TI AND DI EVENTS

We obtain the TI and DI events with a code that incorporates the formulation of the ECBB model described in Sec. II C and a code that incorporates the formulation of the H model described in Sec. II B. Once we obtain these events, we perform a detailed analysis with a different set of codes. In both analysis codes, i.e., one for each model, we use the framework we developed in Sec. II C 5 to determine on the fly during propagation if an electron is quasifree or bound. We register a TI or DI event as direct if a recollision is associated with the simultaneous ionization of three or two electrons. We take the following steps to identify direct events:

(1) We find the ionization time of each electron, $t_{\rm ion}^i$, with $i = 1, 2, 3$ for TI and $i = 1, 2$ for DI.

(2) We register the maxima in the interelectronic potential energies as a function of time between electron pairs i, j and i, k and j, k during the time intervals when in these pairs one electron is quasifree and the other is bound. Next, for each electron i, we identify the maximum for each one of the i, j and i, k potential energies that is closest to the time $t_{\rm ion}^i$. We denote these times as $t_{\rm rec}^{i,j}$ and $t_{\rm rec}^{i,k}$. We obtain at most six such times for TI events and four for DI events.

(3) For each time $t_{\rm rec}^{i,j}$ we identify the time t_2 (see Sec. II C 5) of closest approach to the core of the quasifree electron (either electron i or j) that is closest to $t_{\rm rec}^{i,j}$ and denote it as $t_2^{i,j}$. We obtain at most six such times for TI events and four for DI events.

We label a TI event as direct if four of the times $t_2^{i,j}$ are the same, accounting for one electron being quasifree and the other two bound. That is, if electron i is quasifree during the recollision closest to the ionization time $t_{\rm ion}^i$ then the times $t_2^{i,j}$, $t_2^{i,k}$, $t_2^{j,i}$, and $t_2^{k,i}$ should be the same. The times $t_2^{j,i}$ and $t_2^{k,i}$ are associated with the recollision times $t_{\rm rec}^{j,i}$ and $t_{\rm rec}^{k,i}$ for the bound electrons j and k, respectively. For the quasifree electron we obtain two recollision times $t_{\rm rec}^{i,j}$ and $t_{\rm rec}^{i,k}$ associated with the ionization time $t_{\rm ion}^i$. We choose the one that has the largest difference from t_{ion}^i, guaranteeing a stricter criterion for direct TI events. Next, we check whether $|t_{\rm rec}^{i,j} - t_{\rm ion}^i| < t_{\rm diff}$ or $(t_{\rm ion}^i < t_{\rm rec}^{i,j}$ and $t_{\rm ion}^i < t_{\rm rec}^{i,k})$ and $|t_{\rm rec}^{j,i} - t_{\rm ion}^j| < t_{\rm diff}$ and $|t_{\rm rec}^{k,i} - t_{\rm ion}^k| < t_{\rm diff}$. If the latter conditions

are satisfied then we label the event as direct TI. The condition ($t^i_{\rm ion} < t^{i,j}_{\rm rec}$ and $t^i_{\rm ion} < t^{i,k}_{\rm rec}$) has also been used in our previous studies [35,65] to account for a quasifree electron ionizing significantly earlier before recollision. This happens mostly at high intensities. A similar process is followed to identify a DI event.

The interval $t_{\rm diff}$ is defined as the time duration where the interelectronic potential energy undergoes a sharp change due to recollision. For the laser field intensities considered in this work, we find $t_{\rm diff}$ to be roughly equal to 1/8 laser cycle (T) for the ECBB model and 1/6 T for the H model. The difference in $t_{\rm diff}$ between the two models is due to the stronger electron-core interaction for the ECBB model resulting in sharper changes to the electron-electron interaction. The choice of $t_{\rm diff}$ does not significantly change the percentage contribution of direct TI and DI events [35].

[1] J. S. Parker, L. R. Moore, D. Dundas, and K. T. Taylor, Double ionization of helium at 390 nm, J. Phys. B: At. Mol. Opt. Phys. **33**, L691 (2000).

[2] J. S. Parker, B. J. S. Doherty, K. T. Taylor, K. D. Schultz, C. I. Blaga, and L. F. DiMauro, High-Energy Cutoff in the Spectrum of Strong-Field Nonsequential Double Ionization, Phys. Rev. Lett. **96**, 133001 (2006).

[3] A. Zielinski, V. P. Majety, and A. Scrinzi, Double photoelectron momentum spectra of helium at infrared wavelength, Phys. Rev. A **93**, 023406 (2016).

[4] G. S. J. Armstrong, D. D. A. Clarke, J. Benda, J. Wragg, A. C. Brown, and H. W. van der Hart, Enhancing spin polarization using ultrafast angular streaking, Phys. Rev. A **103**, 053123 (2021).

[5] L.-B. Fu, J. Liu, J. Chen, and S.-G. Chen, Classical collisional trajectories as the source of strong-field double ionization of helium in the knee regime, Phys. Rev. A **63**, 043416 (2001).

[6] L.-B. Fu, J. Liu, and S.-G. Chen, Correlated electron emission in laser-induced nonsequence double ionization of helium, Phys. Rev. A **65**, 021406(R) (2002).

[7] A. Emmanouilidou, Recoil collisions as a portal to field-assisted ionization at near-uv frequencies in the strong-field double ionization of helium, Phys. Rev. A **78**, 023411 (2008).

[8] K. Sacha and B. Eckhardt, Nonsequential triple ionization in strong fields, Phys. Rev. A **64**, 053401 (2001).

[9] J. Guo and X.-S. Liu, Lithium ionization by an intense laser field using classical ensemble simulation, Phys. Rev. A **78**, 013401 (2008).

[10] P. J. Ho and J. H. Eberly, In-Plane Theory of Nonsequential Triple Ionization, Phys. Rev. Lett. **97**, 083001 (2006).

[11] Y. Zhou, Q. Liao, and P. Lu, Complex sub-laser-cycle electron dynamics in strong-field nonsequential triple ionization, Opt. Express **18**, 16025 (2010).

[12] Q. Tang, C. Huang, Y. Zhou, and P. Lu, Correlated multielectron dynamics in mid-infrared laser pulse interactions with neon atoms, Opt. Express **21**, 21433 (2013).

[13] P. J. Ho and J. H. Eberly, Argon-like three-electron trajectories in intense-field double and triple ionization, Opt. Express **15**, 1845 (2007).

[14] J. H. Thiede, B. Eckhardt, D. K. Efimov, J. S. Prauzner-Bechcicki, and J. Zakrzewski, *Ab initio* study of time-dependent dynamics in strong-field triple ionization, Phys. Rev. A **98**, 031401(R) (2018).

[15] J. S. Prauzner-Bechcicki, D. K. Efimov, M. Mandrysz, and J. Zakrzewski, Strong-field triple ionisation of atoms with p^3 valence shell, J. Phys. B: At. Mol. Opt. Phys. **54**, 114001 (2021).

[16] D. K. Efimov, A. Maksymov, M. Ciappina, J. S. Prauzner-Bechcicki, M. Lewenstein, and J. Zakrzewski, Three-electron correlations in strong laser field ionization, Opt. Express **29**, 26526 (2021).

[17] H. Jiang and F. He, Semiclassical study of nonsequential triple ionization of Ar in strong laser fields, Phys. Rev. A **104**, 023113 (2021).

[18] R. Moshammer, B. Feuerstein, W. Schmitt, A. Dorn, C. D. Schröter, J. Ullrich, H. Rottke, C. Trump, M. Wittmann, G. Korn, K. Hoffmann, and W. Sandner, Momentum Distributions of Ne^{n+} Ions Created by an Intense Ultrashort Laser Pulse, Phys. Rev. Lett. **84**, 447 (2000).

[19] A. Rudenko, T. Ergler, K. Zrost, B. Feuerstein, V. L. B. de Jesus, C. D. Schröter, R. Moshammer, and J. Ullrich, From non-sequential to sequential strong-field multiple ionization: Identification of pure and mixed reaction channels, J. Phys. B: At. Mol. Opt. Phys. **41**, 081006 (2008).

[20] N. Ekanayake, S. Luo, B. L. Wen, L. E. Howard, S. J. Wells, M. Videtto, C. Mancuso, T. Stanev, Z. Condon, S. LeMar, A. D. Camilo, R. Toth, W. B. Crosby, P. D. Grugan, M. F. Decamp, and B. C. Walker, Rescattering nonsequential ionization of Ne^{3+}, Ne^{4+}, Ne^{5+}, Kr^{5+}, Kr^{6+}, Kr^{7+}, and Kr^{8+} in a strong, ultraviolet, ultrashort laser pulse, Phys. Rev. A **86**, 043402 (2012).

[21] O. Herrwerth, A. Rudenko, M. Kremer, V. L. B. de Jesus, B. Fischer, G. Gademann, K. Simeonidis, A. Achtelik, T. Ergler, B. Feuerstein, C. D. Schröter, R. Moshammer, and J. Ullrich, Wavelength dependence of sub-laser-cycle few-electron dynamics in strong-field multiple ionization, New J. Phys. **10**, 025007 (2008).

[22] K. Zrost, A. Rudenko, T. Ergler, B. Feuerstein, V. L. B. de Jesus, C. D. Schröter, R. Moshammer, and J. Ullrich, Multiple ionization of Ne and Ar by intense 25 fs laser pulses: Few-electron dynamics studied with ion momentum spectroscopy, J. Phys. B: At. Mol. Opt. Phys. **39**, S371 (2006).

[23] A. Rudenko, K. Zrost, B. Feuerstein, V. L. B. de Jesus, C. D. Schröter, R. Moshammer, and J. Ullrich, Correlated Multielectron Dynamics in Ultrafast Laser Pulse Interactions with Atoms, Phys. Rev. Lett. **93**, 253001 (2004).

[24] H. Shimada, Y. Nakai, H. Oyama, K. Ando, T. Kambara, A. Hatakeyama, and Y. Yamazaki, Recoil-ion momentum spectroscopy of multiply charged argon ions produced by intense ($\sim 10^{16}$ W cm^{-2}) laser light, Nucl. Instrum. Methods Phys. Res. Sect. B **235**, 221 (2005).

[25] A. Emmanouilidou and J. M. Rost, The Coulomb four-body problem in a classical framework: Triple photoionization of lithium, J. Phys. B: At. Mol. Opt. Phys. **39**, 4037 (2006).

[26] A. Emmanouilidou, P. Wang, and J. M. Rost, Initial State Dependence in Multielectron Threshold Ionization of Atoms, Phys. Rev. Lett. **100**, 063002 (2008).

[27] J. Colgan and M. S. Pindzola, Angular Distributions for the Complete Photofragmentation of the Li Atom, Phys. Rev. Lett. **108**, 053001 (2012).

[28] J. Colgan, A. Emmanouilidou, and M. S. Pindzola, Evidence for a T-Shape Break-Up Pattern in the Triple Photoionization of Li, Phys. Rev. Lett. **110**, 063001 (2013).

[29] C. L. Kirschbaum and L. Wilets, Classical many-body model for atomic collisions incorporating the Heisenberg and Pauli principles, Phys. Rev. A **21**, 834 (1980).

[30] J. S. Cohen, Quasiclassical effective Hamiltonian structure of atoms with $Z = 1$ to 38, Phys. Rev. A **51**, 266 (1995).

[31] J. S. Cohen, Quasiclassical-trajectory Monte Carlo methods for collisions with two-electron atoms, Phys. Rev. A **54**, 573 (1996).

[32] V. J. Montemayor and G. Schiwietz, Dynamic target screening for two-active-electron classical-trajectory Monte Carlo calculations for $\mathbf{H}^+ +$ He collisions, Phys. Rev. A **40**, 6223 (1989).

[33] M. B. Peters, V. P. Majety, and A. Emmanouilidou, Triple ionization and frustrated triple ionization in triatomic molecules driven by intense laser fields, Phys. Rev. A **103**, 043109 (2021).

[34] L. Sarkadi, Comparative study of classical theoretical descriptions of the ionization of atoms induced by few-cycle laser pulses, Phys. Rev. A **103**, 053113 (2021).

[35] A. Chen, M. Kübel, B. Bergues, M. F. Kling, and A. Emmanouilidou, Non-sequential double ionization with near-single cycle laser pulses, Sci. Rep. **7**, 7488 (2017).

[36] A. Staudte, C. Ruiz, M. Schöffler, S. Schössler, D. Zeidler, T. Weber, M. Meckel, D. M. Villeneuve, P. B. Corkum, A. Becker, and R. Dörner, Binary and Recoil Collisions in Strong Field Double Ionization of Helium, Phys. Rev. Lett. **99**, 263002 (2007).

[37] A. Rudenko, V. L. B. de Jesus, T. Ergler, K. Zrost, B. Feuerstein, C. D. Schröter, R. Moshammer, and J. Ullrich, Correlated Two-Electron Momentum Spectra for Strong-Field Nonsequential Double Ionization of He at 800 nm, Phys. Rev. Lett. **99**, 263003 (2007).

[38] D. F. Ye, X. Liu, and J. Liu, Classical Trajectory Diagnosis of a Fingerlike Pattern in the Correlated Electron Momentum Distribution in Strong Field Double Ionization of Helium, Phys. Rev. Lett. **101**, 233003 (2008).

[39] M. Verschl and C. H. Keitel, Relativistic recollisions with two consecutive laser pulses, J. Phys. B: At. Mol. Opt. Phys. **40**, F69 (2007).

[40] E. Lötstedt and K. Midorikawa, Effect of the laser magnetic field on nonsequential double ionization of He, Li^+, and Be^{2+}, Phys. Rev. A **87**, 013426 (2013).

[41] P. D. Grugan, S. Luo, M. Videtto, C. Mancuso, and B. C. Walker, Classical study of ultrastrong nonperturbative-field interactions with a one-electron atom: Validity of the dipole approximation for the bound-state interaction, Phys. Rev. A **85**, 053407 (2012).

[42] H. Price, C. Lazarou, and A. Emmanouilidou, Toolkit for semi-classical computations for strongly driven molecules: Frustrated ionization of H_2 driven by elliptical laser fields, Phys. Rev. A **90**, 053419 (2014).

[43] G. P. Katsoulis, M. B. Peters, A. Staudte, R. Bhardwaj, and A. Emmanouilidou, Signatures of magnetic-field effects in non-sequential double ionization manifesting as backscattering for molecules versus forward scattering for atoms, Phys. Rev. A **103**, 033115 (2021).

[44] P. Pihajoki, Explicit methods in extended phase space for inseparable Hamiltonian problems, Celest. Mech. Dyn. Astron. **121**, 211 (2015).

[45] L. Liu, X. Wu, G. Huang, and F. Liu, Higher order explicit symmetric integrators for inseparable forms of coordinates and momenta, Mon. Not. R. Astron. Soc. **459**, 1968 (2016).

[46] W. H. Press, S. A. Teukolsky, W. T. Vetterling, and B. P. Flannery, *Numerical Recipes: The Art of Scientific Computing*, 3rd ed. (Cambridge University Press, Cambridge, UK, 2007)

[47] R. Bulirsch and J. Stoer, Numerical treatment of ordinary differential equations by extrapolation methods, Numer. Math. **8**, 1 (1966).

[48] D. H. Kobe and K-H. Yang, Energy of a classical charged particle in an external electromagnetic field, Eur. J. Phys. **8**, 236 (1987).

[49] E. Yakaboylu, M. L. Klaiber, H. Bauke, K. Z. Hatsagortsyan, and C. H. Keitel, Relativistic features and time delay of laser-induced tunnel ionization, Phys. Rev. A **88**, 063421 (2013).

[50] D. C. Heggie, A global regularisation of the gravitational N-body problem, Celest. Mech. **10**, 217 (1974).

[51] J. G. Leopold and I. C. Percival, Ionisation of highly excited atoms by electric fields. III. Microwave ionisation and excitation, J. Phys. B: At. Mol. Opt. Phys. **12**, 709 (1979).

[52] L. D. Landau and E. M. Lifshitz, *Quantum Mechanics: Non-Relativistic Theory*, Vol. 3 (Elsevier, Amsterdam, 2013).

[53] N. B. Delone and V. P. Krainov, Energy and angular electron spectra for the tunnel ionization of atoms by strong low-frequency radiation, J. Opt. Soc. Am. B **8**, 1207 (1991).

[54] R. Y. Rubinstein and D. P. Froese, *Simulation and the Monte Carlo Method* (Wiley, New York, 2016).

[55] B. HuP, J. Liu, and S.-G Chen, Plateau in above-threshold-ionization spectra and chaotic behavior in rescattering processes, Phys. Lett. A **236**, 533 (1997).

[56] N. B. Delone and V. P. Krainov, Tunneling and barrier-suppression ionization of atoms and ions in a laser radiation field, Phys.-Usp. **41**, 469 (1998).

[57] L. Fechner, N. Camus, J. Ullrich, T. Pfeifer, and R. Moshammer, Strong-Field Tunneling from a Coherent Superposition of Electronic States, Phys. Rev. Lett. **112**, 213001 (2014).

[58] Y. Zhou, C. Huang, Q. Liao, and P. Lu, Classical Simulations Including Electron Correlations for Sequential Double Ionization, Phys. Rev. Lett. **109**, 053004 (2012).

[59] Y. Zhou, Q. Zhang, C. Huang, and P. Lu, Classical description of strong-field double ionization by elliptical laser pulses, Phys. Rev. A **86**, 043427 (2012).

[60] A. Tong, Y. Zhou, and P. Lu, Resolving subcycle electron emission in strong-field sequential double ionization, Opt. Express **23**, 15774 (2015).

[61] C. O. Reinhold and C. A. Falcón, Classical ionization and charge-transfer cross sections for $H^+ +$ He and $H^+ + Li^+$ collisions with consideration of model interactions, Phys. Rev. A **33**, 3859 (1986).

[62] P. B. Corkum, Plasma Perspective on Strong Field Multiphoton Ionization, Phys. Rev. Lett. **71**, 1994 (1993).

[63] A. Emmanouilidou, J. S. Parker, L. R. Moore, and K. T. Taylor, Direct versus delayed pathways in strong-field non-sequential double ionization, New J. Phys. **13**, 043001 (2011).

[64] P. Wang, A. M. Sayler, K. D. Carnes, B. D. Esry, and I. Ben-Itzhak, Disentangling the volume effect through intensity-difference spectra: Application to laser-induced dissociation of H_2^+, Opt. Lett. **30**, 664 (2005).

[65] G. P. Katsoulis, A. Hadjipittas, B. Bergues, M. F. Kling, and A. Emmanouilidou, Slingshot Nonsequential Double Ionization as a Gate to Anticorrelated Two-Electron Escape, Phys. Rev. Lett. **121**, 263203 (2018).